

RESEARCH ARTICLE

ENRICHMENT IN A STOICHIOMETRIC MODEL OF TWO PRODUCERS AND ONE CONSUMER

LAURENCE HAO-RAN LIN^{a,◊}, BRUCE B. PECKHAM^{a,**}, HARLAN W. STECH^{a,†},
and JOHN PASTOR^{b,‡}

^a*Department of Mathematics and Statistics, University of Minnesota, Duluth MN 55812;
Dept. Fax: 218-726-8399;*

^b*Department of Biology, University of Minnesota, Duluth MN 55812; Dept. Fax: 218-726-8142;*

*Email: linx0275@d.umn.edu, Contact Phone: 218-349-3782

**Email: bpeckham@d.umn.edu, Office Phone: 218-726-6188

†Email: hstech@d.umn.edu, Office Phone: 218-726-8272

‡Email: jpastor@d.umn.edu, Office Phone: 218-726-7001

(v1.0 released June 2009)

We consider a stoichiometric population model of two producers and one consumer. It is a generalization of the Rosenzweig-MacArthur population growth model, which is a one-producer, one-consumer population model without stoichiometry. The generalization involves two independent steps: 1) introducing stoichiometry into the system by considering food quality (nutrient) in addition to food quantity (carbon), and 2) adding a second producer which competes with the first. The model is open for carbon but closed for nutrient. Both generalization steps introduce additional equilibria and bifurcations to those of the Rosenzweig-MacArthur model.

The focus of this paper is on the bifurcations which are the result of enrichment. The primary parameters we vary are the growth rates of both producers. Secondary variable parameters are the total nutrient in the system, and the producer nutrient uptake rates. The possible equilibria are: no-life, one-producer, coexistence of both producers, the consumer coexisting with either producer, and the consumer coexisting with both producers. We observe limit cycles in the latter three coexistence combinations. Bifurcation diagrams along with corresponding representative time series summarize the behaviors observed for this model.

Keywords: Population model, producer-consumer, predator-prey, stoichiometry, bifurcation, enrichment

1. Introduction

A population is the collection of inter-breeding organisms of a particular species. Mathematical population models follow the size of interacting populations over time. Such models are fundamental in biology and ecology. A producer-consumer (prey-predator) population model studies the populations of two species which interact in a specific way. A variety of producer-consumer models has been developed and studied over the last century, usually with a single currency, such as biomass, for each population. More recently, stoichiometry, which can be thought as tracking food quality as well as quantity, has been introduced into population models [1, 2, 7, 10, 14, 15, 24–28, 30, 39–41, 44, 45].

◊Corresponding author. Email: linx0275@d.umn.edu, laurenl@vt.edu

In this paper we track carbon and one additional “generic” nutrient. Food that has a low stoichiometric ratio – nutrient to carbon – is considered to be of low quality, and contributes less to consumer growth than high ratio food.

As background for our model, we review the Rosenzweig and MacArthur model from 1963 [37]. They presented a geometric analysis of producer growth and consumer response. It has become one of the classic producer-consumer population models with a single currency (i.e., no stoichiometry). Formulas (1) are a standard realization of the Rosenzweig-MacArthur model, using logistic producer growth and Holling Type II consumer response, with food saturation.

$$\begin{cases} \frac{dP}{dt} = rP - \lambda P^2 - f(P)C \\ \frac{dC}{dt} = \gamma f(P)C - dC \\ f(P) = \frac{\alpha P}{h+P} \end{cases} \quad (1)$$

r is the maximal per-capita growth rate of producer λ is the producer self-limitation coefficient.

γ is the efficiency of turning predated food into consumer biomass.

d is the per-capita death rate of the consumer.

$f(P)$ is a Holling Type II function that describes consumer food saturation.

α is the maximal producer death rate per consumer encounter due to predation.

h is the half-saturation constant for the Holling Type II function.

A standard parameter to vary in (1) is the producer growth rate r . For low r the model predicts a producer monoculture system because there is not enough food to maintain the consumer. Increasing r sufficiently to pass a transcritical bifurcation value allows both producer and consumer to stably coexist. Further increase in r results in a destabilization of the coexistence equilibrium in a Hopf bifurcation, accompanied by the birth of an attracting limit cycle. The amplitude of the cycle grows with continuing increase in r , but no further bifurcations are observed [43].

We build our model from the Rosenzweig-MacArthur model by adding a second producer which competes with the first, and by introducing stoichiometry by lowering the rate of biomass conversion from the producers to the consumer when the nutrient to carbon ratio of the food (producers) is below the level needed for consumer biomass creation. We keep track of both carbon (as a surrogate for biomass) and a nutrient. Our system is assumed to be open for carbon, but closed for nutrient. Like most nutrient models, we track nutrient in the sediment as well as in the two producers and the consumer. More details are provided in Section 2.

Although there are many parameters in our model, we focus on enrichment parameters. We vary two “primary” parameters: the growth rates of the two producers. Secondly, we vary the total nutrient available in the system, and the nutrient uptake rates for the producer(s). We perform a bifurcation study using

a combination of analysis and numerics. As in other stoichiometric models with closed nutrient cycles, our model exhibits a “paradox of energy enrichment.” This is a phenomenon in which the population of the consumer declines in response to an increase in the population of the producer [7, 24, 26, 41, 44]. The paradox of enrichment is one of several ways in which the system can go from parameter combinations allowing coexistence of all three species to parameter combinations where at least one of the three species fails to survive. Identifying these transitions, which turn out to all be some version of a transcritical bifurcation, is a significant contribution of this study.

The papers which match our model assumptions most closely – but for one producer instead of two – are Loladze, Kuang, and Elser (LKE) [26], Kuang, Huisman and Elser (KHE) [24], and Wang, Kuang, and Loladze (WKL) [44]. The LKE model does not include a separate nutrient pool. The KHE and WKL models do include a nutrient pool. All three models are closed for nutrient, and have stoichiometric limitation for conversion from producer to consumer that is similar to ours. All three models have nutrient uptake assumptions that differ from ours. Additionally, their models all include stoichiometric limitation for producer growth. All three studies examine system behavior under enrichment, but the enrichment is effected by directly increasing producer carrying capacity, rather than increasing producer growth rates.

Miller, Kuang, Fagan and Elser [28] investigate a model which, like ours, has two producers, one consumer and stoichiometry. Their model differs from ours in several facets, most significantly in that they assume the two producers are in different patches, and that available nutrient for uptake (rather than total nutrient) remains constant. Andersen [1] includes a model which also has two producers, one consumer and stoichiometry, but it also differs in many ways from our model. Most significantly, the Anderson study considers open nutrient systems (chemostats), while ours is closed. The Anderson model does not assume any competition or self limitation between producers, and it makes different assumptions regarding nutrient uptake by the producers. Further, our interests are in examining enrichment-induced changes in system dynamics – a topic not considered in [1]. Grover [14, 15] also considers stoichiometric chemostat models with competing producers and a consumer.

There are numerous papers considering competing producers and a consumer along with a resource which limits producer growth, but do not limit conversion efficiency [13, 16, 21, 23, 33]. For other two-producer, one-consumer models, but without stoichiometry, see [11, 42]. See [17] for a more mechanistic model of competing producers, but without a consumer and without stoichiometry.

The paper is organized as follows. In section 2 we provide the details of the model construction. In section 3 we analyze the “reduced” model, having a consumer with only one producer. This lays the groundwork for the techniques used in section 4 to analyze the full model. The analysis of the reduced model also provides a basis of comparison for the full model. Discussion is in section 5, and conclusions in section 6.

2. Model Construction

This model contains two producer populations, a single consumer population, and a sediment compartment. We have made the model sufficiently general to apply to a variety of population scenarios, both terrestrial and aquatic. We assume that the stoichiometry plays a role only in the conversion of biomass from producer to consumer. This is appropriate for nutrients that are limiting for the consumer, but not for the producers. As examples, terrestrial systems might include moose or elk consuming two different types of plants for calcium or sodium. These nutrients are required for the moose, but neither limits producer growth [4, 9, 29]. Aquatic systems might include *Daphnia* consuming two different types of algae, with any of lithium, rubidium, strontium, bromine, or iodine as the essential nutrient [20]. None of these nutrients is essential for algal growth. The model is also applicable to algae/*Daphnia* systems with nitrogen or phosphorus as the nutrient. In this case, however, if the nutrient is limiting to the algae as well as the *Daphnia*, our model must be considered as an approximation to the full system, allowing us to focus on the specific role of stoichiometry in the conversion of food from the producers to the consumer. See [26, 44], for example, for algae/*Daphnia* models where stoichiometry is assumed to limit the growth of both the consumer and the producers.

We choose to keep track of carbon density as a measure of biomass quantity, and nutrient density (later changed to the nutrient-to-carbon ratio) as a measure of food quality. This leads to three carbon variables: P_1 , P_2 , C , and four nutrient variables: N_1 , N_2 , N_C , M , where M denotes the mineralized nutrient concentration in the sediment. Variables of the model are summarized in table 1. The model we will actually study is reduced from these seven variables to five by assuming a fixed amount of total nutrient, and a fixed stoichiometric ratio $q = N_C/C$ for the consumer. The latter reduction is justified since stoichiometric ratios tend to be relatively constant for most animals, but have been observed to have a wider range of values for plants [39]. Figure 1 illustrates the flow of carbon and cycle of nutrient in the model.

The equations for our model are given below in equation (2).

$$\begin{cases} \frac{dP_1}{dt} = g_1(P_1, P_2)P_1 - d_{p_1}P_1 - \frac{P_1}{P_1+P_2} \frac{\alpha(P_1+P_2)}{h+(P_1+P_2)} C \\ \frac{dP_2}{dt} = g_2(P_1, P_2)P_2 - d_{p_2}P_2 - \frac{P_2}{P_1+P_2} \frac{\alpha(P_1+P_2)}{h+(P_1+P_2)} C \\ \frac{dC}{dt} = \min\{\gamma, \frac{1}{q} \frac{N_1+N_2}{P_1+P_2}\} \frac{\alpha(P_1+P_2)}{h+(P_1+P_2)} C - d_c C \\ \frac{dN_1}{dt} = \beta_1(N_T - qC - N_1 - N_2)g_1(P_1, P_2)P_1 - \frac{P_1}{P_1+P_2} \frac{\alpha(P_1+P_2)}{h+(P_1+P_2)} C \frac{N_1}{P_1} - d_{p_1}N_1 \\ \frac{dN_2}{dt} = \beta_2(N_T - qC - N_1 - N_2)g_2(P_1, P_2)P_2 - \frac{P_2}{P_1+P_2} \frac{\alpha(P_1+P_2)}{h+(P_1+P_2)} C \frac{N_2}{P_2} - d_{p_2}N_2 \end{cases} \quad (2)$$

where the producer per capita growth functions we use are $g_1(P_1, P_2) = \max\{(b_1 - \lambda_{11}P_1 - \lambda_{12}P_2), 0\}$ and $g_2(P_1, P_2) = \max\{(b_2 - \lambda_{22}P_2 - \lambda_{21}P_1), 0\}$.

We now describe the specific assumptions which lead to equations (2).

Carbon flow: P_1, P_2, C .

Carbon is fixed in the producers due to photosynthesis. This producer growth is assumed to be logistic. Producer respiration, not explicitly modeled, is as-

sumed to be a constant fraction of the carbon fixation. That is, the per capita growth terms ($b_i P_i - \lambda_{ii} P_i^2 - \lambda_{ij} P_i P_j$) are interpreted as “net photosynthesis.” Lotka-Volterra competition is assumed between the two producers. Competition is assumed to be “weak”: the product of the competition coefficients $\lambda_{12}\lambda_{21}$ is assumed to be always less than the product of the self-limitation coefficients $\lambda_{11}\lambda_{22}$. This allows coexistence of the two producers in the absence of the consumer whenever the producer growth rates are sufficiently close to each other [3, 32]. We assume that the nutrient limits only consumer conversion, but not producer growth. Because we assume nutrient uptake depends on producer growth, a reduction in growth rate is not the same as an increase in the death rate. Consequently, the producer death terms ($d_{P_i} P_i$) are separated from the growth terms in our model, and the growth terms are taken to be nonnegative. This is why we use the “max” function in defining g_i , the producer per capita growth functions.

We assume the amount of carbon in the sediment does not affect any of the other variables, so there is no need to include a carbon sediment compartment in the model. Mortality results in an exit of carbon, but not nutrient, from the system. See Fig. 1.

The predation of both producers (consumer response) is assumed to follow a Holling type II function. Both producers are food for the consumer, which forages nonpreferentially: the probabilities of producer P_1 and P_2 being eaten are assumed to be $\frac{P_1}{P_1+P_2}$ and $\frac{P_2}{P_1+P_2}$, respectively. That is, the producers are consumed in proportion to their relative abundance.

The consumer gains biomass through predation. The biomass conversion efficiency is modelled as the minimum of γ and $\frac{N_1+N_2}{q(P_1+P_2)}$, the ratio of the aggregate food source’s stoichiometry, $\frac{N_1+N_2}{P_1+P_2}$, to the consumer’s stoichiometry, q . If the food source contains sufficient nutrient to support the maximum conversion efficiency γ , then the rate γ is achieved. Otherwise, stoichiometric limitation reduces the conversion efficiency to $\frac{N_1+N_2}{q(P_1+P_2)}$, reflecting the maximum rate at which nutrient can be supplied to build structural consumer biomass. Implicit in the use of this term is the assumption that the consumer assimilates a mixture of the two producers together, rather than eating and assimilating one producer at a time. This assumption is similar to the foraging and biomass conversion assumptions in Andersen [1], but differs from those of [28]. The fraction of carbon that is predated, but not assimilated by the consumer, is assumed to exit from the system. The exit can be considered a combination of energy loss and excretion. Note that if the efficiency minimum function is replaced with the constant γ , then the carbon equations decouple from the nutrient equations, and the system reverts to a non-stoichiometric one. Consumer death is assumed to be proportional to its population size.

Nutrient cycling: N_1, N_2 .

The nutrient is assumed to cycle through the four compartments, N_1, N_2, N_C , and M , as in Fig. 1. We eliminate N_C by assuming that the consumer nutrient to carbon ratio is constant q . So $N_C = qC$. Additionally, we eliminate M by assuming a closed nutrient system with total nutrient N_T , so $M = N_T - N_1 - N_2 - qC$. This leaves us with the two nutrient variables N_1 and N_2 .

The producer gains nutrient via uptake from the mineralized nutrient, and loses nutrient due to predation and mortality. The nutrient uptake rate in this model is proportional to the mineralized nutrient $M = N_T - N_1 - N_2 - qC$. In contrast to most other stoichiometric models, nutrient uptake is assumed, as in [17], to be proportional to producer growth, rather than proportional to nutrient density. Of course, proportional uptake would be required of producers that maintain a constant $N : C$ ratio. The nutrient uptake coefficients β_1 and β_2 are assumed to be constant. Nutrient is transferred from producer to consumer via predation, and returned to the nutrient pool when either a producer or the consumer dies. When the producer is nutrient-rich – with nutrient to carbon ratio greater than γ – the consumer does not use all the producer nutrient it consumes. The excess is assumed to be returned to the nutrient pool via excretion. We assume that litter decomposition and nutrient mineralization are instantaneous, so the nutrient is available (in compartment M) for uptake as soon as it leaves the producers or the consumer.

Stoichiometric form.

To simplify somewhat the equilibrium analysis of formulas (2), we introduce producer ratios $Q_i = \frac{N_i}{P_i}, i = 1, 2$. Then calculating the derivatives of Q_1 and Q_2 , we get the equivalent “stoichiometric form” of the system:

$$\begin{cases} \frac{dP_1}{dt} = (g_1(P_1, P_2) - d_{P_1} - \frac{\alpha C}{h+(P_1+P_2)})P_1 \\ \frac{dP_2}{dt} = (g_2(P_1, P_2) - d_{P_2} - \frac{\alpha C}{h+(P_1+P_2)})P_2 \\ \frac{dC}{dt} = (\min(\gamma, \frac{1}{q} \frac{P_1 Q_1 + P_2 Q_2}{P_1 + P_2}) \frac{\alpha(P_1 + P_2)}{h+(P_1 + P_2)} - d_c)C \\ \frac{dQ_1}{dt} = (\beta_1(N_T - qC - Q_1 P_1 - Q_2 P_2) - Q_1)g_1(P_1, P_2) \\ \frac{dQ_2}{dt} = (\beta_2(N_T - qC - Q_1 P_1 - Q_2 P_2) - Q_2)g_2(P_1, P_2) \end{cases} \quad (3)$$

where the per capita producer growth functions g_i are given in eq. (2). Note that $\frac{dC}{dt}$ is not defined if both P_1 and P_2 are zero. Assuming $h > 0$, it can, however, be continuously extended to $P_1 = P_2 = 0$ by $\frac{dC}{dt} = -d_c C$, because of the $\frac{\alpha(P_1 + P_2)}{h + P_1 + P_2}$ factor.

Parametrization.

For our numerical investigations, we select the following parameters, representing two nearly identical producer species (differing only in maximal per-capita growth rates b_1 and b_2) and a nutrient-rich (relatively high q) consumer.

- Maximal producer photosynthetic growth rate: $b_i \in [0, 20]$
- Total nutrient density: $N_T \in [0, 0.5]$, default: 0.1
- Self-limiting coefficients: $\lambda_{11} = \lambda_{22} = 0.5$
- Interference coefficients: $\lambda_{12} = \lambda_{21} = 0.2$
- Producer per-capita natural death rates: $d_{P_1} = d_{P_2} = 0.05$
- Consumer per-capita death rate: $d_c = 0.17$
- Consumer stoichiometric ratio: $q = 0.05$
- Maximal biomass conversation efficiency: $\gamma = 0.1$
- Maximal predation rate: $\alpha = 2.75$
- Predation half-saturation coefficients: $h = 0.75$,

Nutrient uptake constants $\beta_1 \in \{0.1, 0.2, 0.3\}$, default: 0.3; $\beta_2 = 0.3$.

Our primary goal is to determine the effects of system enrichment with respect to carbon and nutrients. Increasing b_i is assumed to correspond to carbon enrichment; increasing N_T is assumed to enrich the system with nutrients. Consequently, the parameters, b_1 , b_2 , and N_T are varied in our numerical experiments. We also experiment with different values of β_1 , the first producer's nutrient uptake rate. Rate constants are dependent on the time scale and the units selected to measure biomass and nutrient densities.

Rescalings and alternate parameter selection would likely be necessary to match specific systems. For example, if we rescale both time and the phase variables by a factor of three ($\tilde{t} = 3t, P_1 = 3\tilde{P}_1, P_2 = 3\tilde{P}_2, C = 3\tilde{C}, N_1 = 3\tilde{N}_1, N_2 = 3\tilde{N}_2$) then our variables and parameters are consistent with an algae-*Daphnia* system with rescaled time measured in days, and rescaled phase variables measured in mg/liter [1]. Specifically, the rescalings would result in replacing parameters $b_1, b_2, d_{P_1}, d_{P_2}, \alpha, h, d_C, N_T, \beta_1, \beta_2$ with $b_1/3, b_2/3, d_{P_1}/3, d_{P_2}/3, \alpha/3, h/3, d_C/3, N_T/3, 3\beta_1, 3\beta_2$, respectively. The λ_{ij} 's and γ would remain unchanged. Note that prior stoichiometric algae-*Daphnia* studies [15, 24, 26] have used γ values from 0.65 through 0.8, but other studies suggest a wider range of possible conversion factors, from .01 through 0.8 [6, 18, 19, 36, 38].

3. One-Producer, One-Consumer Model

In order to more easily understand the model (3), we first consider the special case where there is a single producer in the system. We set $P_2 = 0$ and ignore Q_2 . For notational convenience we drop the subscripts from $\lambda_{11}, P_1, Q_1, b_1, \beta_1$ and d_{P_1} for the rest of this section to obtain:

$$\begin{cases} \frac{dP}{dt} = (b - \lambda P - d_P - \frac{\alpha C}{h+P})P \\ \frac{dC}{dt} = (\min(\gamma, \frac{Q}{q}) \frac{\alpha P}{h+P} - d_C)C \\ \frac{dQ}{dt} = ((N_T - qC - QP)\beta - Q)(b - \lambda P) \end{cases} \quad (4)$$

The max function used to define the producer growth rates in (3) is not necessary in (4) as a result of the following Proposition.

Proposition 3.1: *The following inequalities describe a positively invariant region of model (4): $0 \leq P \leq \frac{b}{\lambda}, 0 \leq C \leq \frac{N}{q}, 0 \leq Q \leq N_T\beta$, and $(N_T - qC - QP) \geq 0$.*

Proof: The proof, which is standard for related models in the literature, follows by showing that all solutions which start on the boundary of the region will stay on the boundary or go to the interior of the region. See [25] for details.

□

3.1. Equilibria

We calculate the system equilibria, with the variables listed in the order: (P, C, Q) .

The no-life equilibrium (O): $(0, 0, N_T\beta)$. Neither producer nor consumer exist, but the (irrelevant) producer stoichiometric ratio is not necessarily zero.

The monoculture equilibrium (P): $(\frac{b-d_P}{\lambda}, 0, \frac{N_T\lambda\beta}{\lambda+(b-d_P)\beta})$. In the absence of consumers, the population of producers follows the logistic growth and approaches its carrying capacity $\frac{b-d_P}{\lambda}$ over time.

The coexistence equilibria (PC):

The coexistence equilibria are computed for two cases: that of high food quality (case H), and that of low food quality (case L). We first compute case H equilibrium candidates by replacing $\min(\gamma, \frac{Q}{q})$ with γ in eq. (4). Similarly, we compute case L equilibrium candidates by replacing $\min(\gamma, \frac{Q}{q})$ with $\frac{Q}{q}$. Later we will perform a ‘‘consistency check’’: $\frac{Q}{q} \geq \gamma$ for case H solutions, and $\frac{Q}{q} \leq \gamma$ for case L solutions. Candidate equilibria which satisfy the consistency check will be called *mathematically realized* equilibria. Mathematically realized equilibria with nonnegative coordinates are said to be *ecologically realizable*.

For case H , there is a unique candidate equilibrium, denoted $(PC)_H$. In terms of the parameters, it is $(\frac{d_C h}{\alpha\gamma-d_C}, \frac{h\gamma(b-d_P)}{\alpha\gamma-d_C} - \frac{\gamma d_C \lambda h^2}{(\alpha\gamma-d_C)^2}, \frac{\beta(N_T(\alpha\gamma-d_C) - hq\gamma(b-d_P) + \frac{\lambda\gamma q d_C h^2}{\alpha\gamma-d_C})}{\alpha\gamma-d_C(h\beta-1)})$. Note that the producer equilibrium level is independent of the growth rate b ; increasing b results in increased producer growth, but the growth is balanced by increased consumption by the consumer.

For case L , the candidate coexistence equilibrium set, denoted collectively by $(PC)_L$, is more complicated. By setting the right hand sides of (4) to zero, solving in the third equation for Q , plugging the result into the second equation and solving for C , and substituting these two solutions into the first equation, it can be shown that the equilibria with nonzero P and C must satisfy the following cubic in P .

$$P^3 c_3 + P^2 c_2 + P c_1 + c_0 = 0, \tag{5}$$

where

$$\begin{aligned} c_3 &= -\lambda \\ c_2 &= b - d_P + d_C - h\lambda \\ c_1 &= (b - d_P + d_C)h - \frac{N_T\alpha}{q} + \frac{d_C}{\beta} \\ c_0 &= \frac{hd_C}{\beta} \end{aligned}$$

Thus there can be up to three candidate $(PC)_L$ equilibria. Along with the previous candidate $(PC)_H$ equilibrium, there might exist up to four coexistence equilibria. For the parameter sets we chose, however, we never observed more than three equilibria which simultaneously satisfied the consistency check and were therefore mathematically realized. Fewer still are ecologically realizable since all equilibrium coordinates must be nonnegative. Note that when Q/q is exactly equal to γ , the case H and case L equilibria should coincide.

The stability of equilibria can be determined by computing the associated eigenvalues and checking to see whether all have negative real parts. We do this in our numerical experiments, but we do not provide Jacobian or eigenvalue formulas here.

3.2. Numerical Results

Bifurcations with varying b (maximal per-capita producer productivity) and N_T (total system nutrient) fixed

We provide four views of the same one-parameter bifurcation diagram, varying b , in Fig. 2. The total nutrient N_T is fixed at 0.1. Figures 2(a)-(c) are traditional projections, representing attracting equilibria and limit cycles (max and min) with solid lines, and unstable equilibria with dashed lines. We plot only those equilibria and limit cycle extrema which are ecologically realizable.

Barely visible at this scale is (unlabelled) region O: $0 \leq b \leq d_P = 0.05$, where the growth rate of the producer is insufficient to overcome its natural death rate. The corresponding equilibrium components are plotted in brown. As b increases through 0.05, a transcritical bifurcation leads to a (green) high nutrient producer monoculture, P_H . (The nutrient level of the producer is in some sense irrelevant without a positive level of the consumer since in our model the stoichiometry is only effected through the conversion of biomass in predation. The producer equilibrium, however, can still be classified as high nutrient since $\frac{Q}{q} > \gamma$.) A second transcritical bifurcation at $b \approx 0.65$ allows the transition from the P_H producer monoculture to the (blue) coexistence equilibrium, $(PC)_H$. A Hopf bifurcation at $b \approx 1.63$ produces a stable periodic PC -limit cycle; maximum and minimum values along the periodic cycle (purple) are displayed. The periodic limit cycle is destroyed as a case L saddle-node develops on the cycle at $b \approx 2.6$. We refer to this bifurcation as a “SNIC”, a saddle-node on an invariant circle. The attracting case L coexistence equilibrium $(PC)_L$ (red) born in the saddle-node bifurcation replaces the periodic cycle as the attractor. A “nonsmooth saddle-node” bifurcation separates the two subregions of $(PC)_L$. As we cross the boundary from the left to the right at $b \approx 2.82$, the case H saddle disappears with the case L saddle, leaving the case L attracting equilibrium intact. The nonsmoothness is caused by a crossing of the min function arguments in equation (4). It is also apparent in the “corner” formed where the blue and red dashed equilibrium lines meet. This is in contrast to the quadratic signature of a smooth saddle-node bifurcation.

If the red consumer equilibrium curve in Fig. 2(b) were continued farther out in the parameter b , it would be seen to eventually intersect the b axis at $b \approx 14.14$, resulting in a restabilization of the producer monoculture. This corresponds to entering region P_L in Fig. 3(a). The restabilization of the producer monoculture is a manifestation of the “paradox of energy enrichment,” and appears to be a common feature of stoichiometric models with closed nutrient pools [24, 26, 44]. Recall that the system is open for carbon, whose inputs increase with b , but closed for nutrient. Therefore, increasing b at first increases producer growth, resulting in more food for the consumer, but with lower quality. Once equilibrium $\frac{Q}{q} < \gamma$, food quality controls consumer growth, and continued increase in b enriches the producer(s) with carbon, without any corresponding increase in system

nutrients. Eventually, food quality is too low to allow consumer growth to match consumer death, resulting in consumer extinction and reestablishment of a producer monoculture through a transcritical bifurcation.

Figure 2(d) is an additional bifurcation diagram which is provided to better understand which candidate equilibria are mathematically and/or ecologically realized and which are not. We plot the ratio $\frac{Q}{q}$ at equilibria versus b . This is, of course, merely a rescaled version of Fig. 2(c), but along with the dash-dot reference line at the value of $\gamma = 0.1$, it more directly relates to the min function in equation (4). The linetypes and colors are consistent with Fig. 2(a)-(c). We have added to Fig. 2(d) dotted lines for candidate equilibria which are not mathematically realized. Specifically, the case H equilibrium is realized when it is above γ , and the case L equilibria are realized when they are below γ . Note that in the PC cycle region, the full limit cycle is in case H (above γ) toward the left, but are part in case H and part in case L (below γ) toward the right side of the region. The nonsmooth saddle-node is more clear in Fig. 2(d) as the crossing of the case H and case L equilibria, necessarily at γ .

Figure 2(d) also suggests other possible bifurcation scenarios for alternate choices of our auxiliary parameters (all parameters other than b). For example, if γ were increased above the $\frac{Q}{q}$ value of the unrealized candidate saddle-node at $(b, Q/q) \approx (3.4, 0.2)$, the candidate saddle-node would become a realized saddle-node bifurcation. For γ below the $\frac{Q}{q}$ value of the realized saddle-node (about 0.004), neither case L candidate saddle-node would be realized. If γ , were sufficiently large, 0.7, for example, then for our choice of auxiliary parameters, only case L equilibria will be possible. This leads to bifurcation figures which are qualitatively similar to those in Fig. 2, but with a standard saddle-node bifurcation replacing our nonsmooth saddle-node bifurcation. For other auxiliary parameter choices, the red cubic case L curve could lose its turning points, resulting in the loss of both candidate saddle-nodes. All of these cases have been observed in our numerical experiments.

Table 2 summarizes the attractors in each region and the bifurcations between regions. We note that the sequence of bifurcations in Fig. 2, varying producer growth rate b , is the same as the sequence displayed for the stoichiometric models investigated in LKE, KHE, and WKL [24, 26, 44], where the authors directly vary producer carrying capacity.

Bifurcations with varying b and N_T

To better place the one-parameter bifurcation diagrams in Fig. 2 in context, we show a two-parameter bifurcation diagram in b and N_T in Fig. 3. The solid curves in Fig. 3(a) indicate those bifurcations resulting in a change of attractor; the dashed curves indicate bifurcations which do not change the attractor. The dotted black line corresponds to the $N_T = 0.1$ one parameter cut of Fig. 2. We use color to distinguish bifurcation curve types: blue for transcritical, green for saddle-node, and red for Hopf. Dashed green represents a nonsmooth saddle-node, and dashed black represents a change in classification between case L and case H , but with no accompanying bifurcation. Corresponding time series plots are shown in Fig. 4. In each time series, solutions of P , C , and "magnified"

Q are plotted against time. Table 2 summarizes the bifurcations between the adjacent regions of (b, N_T) parameter space.

Most of the transitions between regions have been described above for the one-parameter cut. The geometry of the regions in the two-parameter plane adds additional insight to the behavior of the model. For example, if we were to take a one-parameter cut with N_T less than about 0.02, then we would never see the consumer persisting. Note that the P_L region extends to the b axis because the producer growth is assumed to be independent of the nutrient availability (recall comments in section 2). If we had included a nutrient requirement for producer growth, then we would expect the region of no growth to extend to a thin L-shaped region next to both axes, rather than just next to the N_T axis. Note also the black dashed lines separating regions P_H from P_L and $(PC)_H$ from $(PC)_L$. The respective regions are distinguished by the producer equilibrium level changing from high nutrient to low nutrient. The dashed green and black lines together are significant because they indicate parameter combinations for which equilibria are located at the nonsmoothness boundary in the phase space.

For comparison, Fig. 3(b) shows a bifurcation diagram of the corresponding model without stoichiometry (replacing $\min(\gamma, \frac{Q}{q})$ with γ). The non-stoichiometric model is, of course, independent of N_T since the model reverts to a single currency model.

4. The Two-Producer, One-Consumer Model

We now turn to an analysis of the full model (3), with both producers, one consumer, and stoichiometry. Much of the analysis parallels that performed in the previous section for a single producer.

Proposition 4.1: *The following inequalities describe a positively invariant region of model (3): $0 \leq P_1 \leq \frac{b_1}{\lambda_{11}}$, $0 \leq P_2 \leq \frac{b_2}{\lambda_{22}}$, $0 \leq C \leq \frac{N_T}{q}$, $0 \leq Q_1 \leq N_T\beta_1$, $0 \leq Q_2 \leq N_T\beta_2$, and $(N_T - qC - Q_1P_1 - Q_2P_2) \geq 0$.*

Proof: The proof is similar to that of Proposition 3.1. See [25] for details.

□

4.1. Equilibria

Equilibria with $P_2 = 0$ and/or $P_1 = 0$ are the same as the equilibria in the single-producer-single-consumer model in the previous section, but with extra “trivial” coordinates. Since Q_i is not ecologically relevant when $P_i = 0$, we denote the corresponding mathematical equilibrium value as being “not applicable” (NA). Coordinates are listed in the order: (P_1, P_2, C, Q_1, Q_2) .

- The no-life equilibrium (O): $(0, 0, 0, \text{NA}, \text{NA})$
- The monoculture equilibrium (P_1): $(\frac{b_1 - d_{P_1}}{\lambda_{11}}, 0, 0, \frac{N_T\beta_1\lambda_{11}}{\lambda_{11} + (b_1 - d_{P_1})\beta_1}, \text{NA})$
- The monoculture equilibrium (P_2): $(0, \frac{b_2 - d_{P_2}}{\lambda_{22}}, 0, \text{NA}, \frac{N_T\beta_2\lambda_{22}}{\lambda_{22} + (b_2 - d_{P_2})\beta_2})$
- The one-producer coexistence equilibrium ($(P_1C)_H$): $(\frac{d_c h}{\gamma\alpha - d_c}, 0, \frac{\gamma h(b_1 - d_{P_1})}{\alpha\gamma - d_c} - \frac{\gamma d_c h^2 \lambda_{11}}{(\alpha\gamma - d_c)^2}, \frac{\beta_1(N_T(\alpha\gamma - d_c) - hq\gamma(b_1 - d_{P_1}) - \frac{d_c q \gamma h^2 \lambda_{11}}{\alpha\gamma - d_c})}{\alpha\gamma - d_c(h\beta_1 - 1)}, \text{NA})$.
- The one-producer coexistence equilibrium ($(P_2C)_H$): $(0, \frac{d_c h}{\gamma\alpha - d_c}, \frac{\gamma h(b_2 - d_{P_2})}{\alpha\gamma - d_c} - \frac{\gamma d_c h^2 \lambda_{22}}{(\alpha\gamma - d_c)^2}, \text{NA}, \text{NA})$.

$$\text{NA, } \left(\frac{\beta_2(N_T(\alpha\gamma - d_c) - hq\gamma(b_2 - d_{P_2}) - \frac{d_c q \gamma h^2 \lambda_{22}}{\alpha\gamma - d_c})}{\alpha\gamma - d_c(h\beta_2 - 1)} \right).$$

The remaining coexistence equilibria involve both producers and are therefore distinct from the equilibria in the single producer analysis. Note that for P_1 and P_2 to be positive equilibrium values, the growth terms $g_i(P_1, P_2)$ must both be positive in equation (3).

- The producer equilibrium without consumer ($P_1 P_2$):

We set $C = 0$ and assume that all other variables are positive. The equilibrium solution is computed to be $(P_1, P_2, C, Q_1, Q_2) =$

$$\left(\frac{\lambda_{22} B_1 - \lambda_{12} B_2}{S_{prod}}, \frac{\lambda_{11} B_2 - \lambda_{21} B_1}{S_{prod}}, 0, \frac{N_T \beta_1 S_{prod}}{B_1(\beta_1 \lambda_{22} - \beta_2 \lambda_{21}) + B_2(\beta_2 \lambda_{11} - \beta_1 \lambda_{12}) + S_{prod}}, \frac{N_T \beta_2 S_{prod}}{B_1(\beta_1 \lambda_{22} - \beta_2 \lambda_{21}) + B_2(\beta_2 \lambda_{11} - \beta_1 \lambda_{12}) + S_{prod}} \right),$$

where $B_1 = b_1 - d_{P_1}$, $B_2 = b_2 - d_{P_2}$, and $S_{prod} = \lambda_{11} \lambda_{22} - \lambda_{12} \lambda_{21}$

In the absence of the consumer, our model reduces to a Lotka-Volterra competition model. Our simplifying assumption that the producer growth be independent of the stoichiometry renders Q_1 and Q_2 irrelevant. It is clear from the first two equations in (3) that in order to have P_1 and P_2 persist at positive levels, we must have $b_1 > d_{P_1}$ and $b_2 > d_{P_2}$. By analyzing nullclines in the P_1 - P_2 plane, it can be shown that to avoid competitive exclusion, we must also require $\frac{b_1 - d_{P_1}}{\lambda_{12}} > \frac{b_2 - d_{P_2}}{\lambda_{22}}$ and $\frac{b_2 - d_{P_2}}{\lambda_{21}} > \frac{b_1 - d_{P_1}}{\lambda_{11}}$. For fixed values of λ_{ij} with λ_{11} and λ_{22} “sufficiently larger” than λ_{12} and λ_{21} , these four inequalities determine a wedge-shaped region in the b_1 - b_2 plane [3, 32]. See wedge $\overline{jrj'}$ in the detailed bifurcation diagram of Figure 9. In words, the growth rates for the two species must be “sufficiently large and close” to allow for coexistence of P_1 and P_2 .

- “Interior” coexistence equilibria (all three species positive):

As we did for the one-producer model, we first calculate all possible *candidate* equilibria. There remain two cases: case H, where $\min(\gamma, \frac{Q_1 P_1 + Q_2 P_2}{q(P_1 + P_2)}) = \gamma$, and case L, where $\min(\gamma, \frac{Q_1 P_1 + Q_2 P_2}{q(P_1 + P_2)}) = \frac{Q_1 P_1 + Q_2 P_2}{q(P_1 + P_2)}$.

- Case H: high food quality coexistence equilibrium $(P_1 P_2 C)_H$:

Assuming all variables are positive, the equilibrium solution is

$$(P_1^*, P_2^*, C^*, \frac{\beta_1(N_T - qC^*)}{1 + \beta_1 P_1^* + \beta_2 P_2^*}, \frac{\beta_2(N_T - qC^*)}{1 + \beta_1 P_1^* + \beta_2 P_2^*}),$$

where $B_1 = b_1 - d_{P_1}$, $B_2 = b_2 - d_{P_2}$,

$$S_{sum} = \lambda_{11} + \lambda_{22} - \lambda_{12} - \lambda_{21},$$

$$S_{prod} = \lambda_{11} \lambda_{22} - \lambda_{12} \lambda_{21},$$

$$P_1^* = \frac{B_1 - B_2}{S_{sum}} + \frac{d_c h (\lambda_{22} - \lambda_{12})}{S_{sum}(\alpha\gamma - d_c)},$$

$$P_2^* = \frac{B_2 - B_1}{S_{sum}} + \frac{d_c h (\lambda_{11} - \lambda_{21})}{S_{sum}(\alpha\gamma - d_c)},$$

$$\text{and } C^* = \frac{\gamma h (B_1(\lambda_{22} - \lambda_{21}) - B_2(\lambda_{11} - \lambda_{12}))}{S_{sum}(\alpha\gamma - d_c)} + \frac{\gamma d_c h^2 S_{prod}}{S_{sum}(\alpha\gamma - d_c)^2}$$

- Case L: low food quality coexistence equilibria $(P_1 P_2 C)_L$:

In this case we assume the $\min(\gamma, \frac{N_1 + N_2}{q(P_1 + P_2)}) = \frac{N_1 + N_2}{q(P_1 + P_2)} = \frac{Q_1 P_1 + Q_2 P_2}{q(P_1 + P_2)}$. The procedure for finding $(P_1 C)_L$ was described in the last section. Similar to the

one-producer, one-consumer model, there are up to three equilibria in the two-producer, one-consumer model. The P_1 equilibrium values for $(P_1P_2C)_L$ can be shown to be the roots of a cubic polynomial [25]. The formula is too complicated to include here, but once a value for P_1 is determined, the remaining four components can then be determined in terms of P_1 .

As in the one-producer reduced model, stability of equilibria can be determined by computing the associated eigenvalues and checking to see whether all have negative real parts. We do this in our numerical experiments, but we do not provide Jacobian or eigenvalue formulas here.

4.2. Numerical results

We computed several bifurcation diagrams to analyze our system. Values of fixed parameters were given in section 2.

Figure 5 contains several bifurcation diagrams summarizing the dynamics and corresponding transitions observed for our set of auxiliary parameters (all parameters except b_1 , and b_2). Figure 5(b) gives an overview for a large range of parameters b_1 and b_2 , and includes the paradox of enrichment regions where the consumer cannot exist for high b_1 and/or b_2 : $(P_1)_{L'}$, $(P_2)_{L'}$, and $(P_1P_2)_{L'}$. Figure 5(a) is an enlargement of Fig. 5(b), showing more detail, and showing all bifurcations which change the attractor. A more complete bifurcation diagram is provided in Fig. 9 in the Appendix. Figure 5(c) is a bifurcation diagram for the analogous two-producer, one-consumer model without stoichiometry (replace $\min(\gamma, \frac{Q_1P_1+Q_2P_2}{q(P_1+P_2)})$ with γ). Comparing Fig. 5(c) with Fig. 5(a) helps to emphasize the impact of including stoichiometry in our model.

We emphasize the “wineglass-shaped” coexistence regions in Fig. 5: a high nutrient equilibrium region $((P_1P_2C)_H)$, a limit cycle region $(P_1P_2C\text{-Cycle})$, and a low nutrient equilibrium region $((P_1P_2C)_L)$. They are separated respectively by a Hopf bifurcation, and a SNIC bifurcation (only in (a) and (b)). Transitions from inside a coexistence region to outside a coexistence region are all transcritical bifurcations, either of equilibria or limit cycles. For our choice of auxiliary parameters, the coexistence region is a subset of the wedge referred to above in the P_1P_2 equilibrium discussion where the two producers coexist in the absence of the consumer. In general, the addition of a consumer to competing species can either facilitate coexistence or hamper it [5, 21, 33]. In our model, the similarity of the two competing species (differing only in growth rates), and the weak competition (compared to self limitation), both cause coexistence to be hampered by the introduction of a consumer. Table 3 summarizes the bifurcations between the adjacent regions. See Fig. 9 in the Appendix for a more detailed version of Fig. 5(a).

Representative time series corresponding to different regions of Fig. 5 are plotted in Fig. 6. Because of the symmetry associated with interchanging P_1 with P_2 , we provide time series for only one of any pair of “conjugate” regions.

Figure 7 illustrates a specific one-parameter cut through Fig. 5(a) and 5(b) at $b_2 = 2.0$. A more detailed explanation is in the Appendix.

Figure 8 provides the results of additional experiments performed by varying

producer nutrient uptake rates. Figure 8(a) shows the two-parameter bifurcation diagram in β and b for the single producer model of section 3. By comparing to the two-parameter bifurcation diagram of Fig. 3(a), it can be seen that increasing the producer nutrient uptake rate is roughly analogous to increasing the total nutrient in the system. Figures 8(b) and 8(c) are analogous to Fig. 5(a), but for unequal values of the producer uptake coefficients β_1 and β_2 . The value of β_2 is fixed at 0.3 in both figures. In Fig. 8(b), β_1 is 0.2, and in Fig. 8(c), β_1 is 0.1. The symmetry of Fig. 5(a) is broken slightly in Fig. 8(b) and more drastically in 8(c). Figure 8(b) is topologically equivalent to Fig. 5(b), but Fig. 8(c) is no longer equivalent. Figure 8(a) helps explain parts of Figs. 8(b) and 8(c) as follows. The horizontal one-parameter cut at $\beta = 0.2$ (respectively $\beta = 0.1$) in Fig. 8(a) corresponds to a horizontal one-parameter cut in Fig. 8(b) (respectively 8(c)) at $b_2 = 0$. Similarly, a one-parameter cut at $\beta = 0.3$ in Fig. 8(a) corresponds to the vertical one-parameter cut in Fig. 8(b) and 8(c) at $b_1 = 0$.

5. Discussion

5.1. Ecological Implications

All the bifurcations described in the preceding sections and associated figures are theoretically relevant to ecological systems, but we emphasize in this section three new behaviors of this model that have interesting ecological implications and which are in principle experimentally testable.

- (1) In a one-producer-consumer system, increasing producer growth rate, b , produces a different sequence of bifurcations and behaviors when the total amount of nutrient, N_T , is low compared to when it is moderate or high (Fig. 3(a)).
- (2) For our choice of auxiliary parameters, the presence of the consumer decreases the region of coexistence of the two producers in the (b_1, b_2) parameter plane (Fig. 9).
- (3) Differential response of producer growth rates (b_i) to enrichment may produce different sequences of bifurcations and species extinctions (Fig. 5(a)).

We have assumed a reasonable set of parameter values for aquatic systems (with rescaling, as indicated at the end of section 2, Model Construction), and different aquatic systems or simple terrestrial systems might be modeled by other parameter selections. However, because the equilibria, their stability, and bifurcation behaviors of the model depend critically on parameter values, it is important in any experimental test to first determine accurate values of the parameters. Standard experimental techniques could be used to establish, for example, producer growth rates b_i , producer nutrient uptake rates β_i , and the reductions in growth rates due to self limitation and interspecies competition (λ_{ij}). Once parameter values have been established for the particular species chosen, then bifurcation diagrams would need to be recomputed to determine the specific values of parameters where transitions are predicted to happen.

To conform to the assumptions of the model, the experimental system must be closed to nutrient fluxes from the outside environment but open to carbon fluxes via producer uptake in photosynthesis and outputs via respiration. A commonly used system which meets these assumptions is a simple aquarium with an initial nutrient pool that remains fixed (but which will be dynamically

allocated amongst the different species) and which is open to carbon fluxes and contains producer(s) such as algae and a consumer such as *Daphnia* or similar zooplankton. See, for example, [8]. In contrast, a chemostat is open to both carbon and nutrients and would not be an appropriate experimental environment.

The general strategy would be to vary experimental conditions to see if the experimental system can be forced across bifurcations, thereby causing a large and observable qualitative change of behavior, such as extinction of one or more species, initiation or quenching of limit cycles, etc. Our simulations suggest that algae-*Daphnia* experiments would need to be run for at least one year to determine periodic behavior and convergence.

The simplest parameter to experimentally vary is the total amount of nutrient, N_T , which can be done by simply fertilizing the system. Species growth rates, b_i , can be varied in two ways: first by judicious choice of different species, secondly by determining whether b_1 and b_2 respond differently to light enrichment because of different photosynthetic response curves for the two producers. (See Urabe and Sterner [41] for an example of altering growth and stoichiometry of algae by augmenting light levels.) Of course, this assumes that b_i is independent of all other parameters, or at most only weakly correlated with them. If the response of b_1 and b_2 can be experimentally established and calibrated to light enrichment, then shading or light augmentation would correspond to a specific path through the (b_1, b_2) plane. Finally, nutrient uptake rates, β_i , can be varied by choice of producer species used in the experiment.

Assuming that these preliminary experimental details can be addressed, the following experiments could test the new behaviors of this model:

- (1) *For the single producer system, bifurcation sequences with increasing producer growth rates will depend on nutrient levels.* In Fig. 3(a), one-parameter cuts in b are qualitatively different at different nutrient levels, N_T . At low nutrient levels (such as $N_T \approx 0.03$ in Fig. 3(a)), as b increases, there is first a transcritical bifurcation where the producer survives without a consumer, a second transcritical bifurcation where the producer and consumer coexist at a stable fixed point equilibrium, and finally at very high producer growth rates the loss of the consumer at another transcritical bifurcation because of very low food quality. This sequence can be tested by increasing b and examining where either species or both exist. In the coexistence region, increase in b should correspond with a decrease in producer nutrient to carbon ratio Q , but sustained high consumer nutrient to carbon ratio (constant in our model at q). When the difference in the ratios is great enough, then the consumer should go extinct. Repeating the experiment at moderate to high nutrient levels (such as $N_T > 0.08$ in Fig. 3(a)) should result in a bifurcation sequence similar to that displayed in Fig. 2, including the birth of a limit cycle via a Hopf bifurcation and the subsequent loss of the limit cycle at higher values of b .
- (2) *The presence of the consumer decreases the region of coexistence of the two producers.* In our model, the two producers can coexist without the consumer because we have assumed weak competition ($\lambda_{ii} > \lambda_{ij}$). If the analogue of Fig. 9 for an experimental system has a three-species coexistence region (the “wineglass”) which is a proper subset of the two-producer coexistence region (the “wedge”), this can be tested by first establishing a microcosm containing two producers which coexist and which have growth

rates which put them within the wedge shaped region of coexistence in the (b_1, b_2) parameter plane but outside the wine glass region of coexistence of two producers and a consumer. Then introduce a suitable consumer who preys on both species. The model of this paper predicts that the producer with the slower growth rate should then go extinct.

- (3) *Differential response of producer growth rates (b_i) to enrichment may produce different sequences of bifurcations and species extinctions* (Fig. 5(a)). Two different producers might respond differently to various sources of carbon enrichment. Therefore, each source of enrichment corresponds to a specific path through the (b_1, b_2) parameter space in Fig. 5(a). For example, suppose the system is known to be at the red dot in region $Cycle_b$ in Fig. 9. If a specific source of enrichment causes b_1 and b_2 to increase at the same rate, we will follow a path of slope one from our starting point. This would result in a straight-forward bifurcation sequence: loss of the interior limit cycle in a SNIC bifurcation, and eventual loss of the consumer in a transcritical bifurcation. On the other hand, another source of enrichment might increase b_1 much more than b_2 . This would result in a path in Fig. 9 that has a slope less than one. This could result in a complicated bifurcation sequence in which, for example, we pass from the interior limit cycle to a P_1C -cycle (region $\{cfnm\}$), to a $(P_1C)_L$ equilibrium (region $\{cmkd\}$), back to coexistence with a $(P_1P_2C)_L$ equilibrium (region $\{acd\}$), out of coexistence again by crossing curve \overline{de} and returning to $(P_1C)_L$, and finally losing the consumer as it crosses from region $(P_1C)_L$ to region $(P_1)_L$. Many other paths are, of course, also possible. This emphasizes the necessity referred to above of recomputing the analogue of the bifurcation diagram in Fig. 5 using the identified parameters for specific species, as well as determining the producer growth rate response to various forms of enrichment. The asymmetries apparent in Fig. 8(c), caused by differing producer nutrient uptake rates, coupled with differing responses of producer growth rates to enrichment, could create further possibilities.

Such experiments would require a careful determination of and precise control over parameter values and probably also virtuoso experimental technique. But if they could be done, then the large and qualitative differences in the sequences of bifurcations, coexistence, and extinctions should prove a useful test of the model presented here.

5.2. Topology versus geometry

The use of bifurcation theory to analyze models has the great advantage of grouping behavior of systems into broad equivalence classes. The mathematical definition of *topological equivalence* of systems of differential equations, however, may be too broad to capture all of the ecological significance of a model. For example, our numerical experiments have resulted in the following geometrically different, but topologically equivalent behavior for “interior” limit cycles. For certain parameter combinations, the limit cycle, starting from small initial conditions for both producers and consumer, exhibits an increase first in one producer, then the second producer, and finally the consumer. As happens in producer-consumer models with a single producer, the growth in consumer leads to a reduction in producer, and then consumer, before returning to the small initial conditions. For different parameter combinations, we observe small initial conditions leading to first the growth of one producer, then the growth of the consumer, and finally the growth of the second producer. Details are in [25]. These two distinct ecological

scenarios are not distinguished by our bifurcation classification.

5.3. Model limitations

There are, of course, many limitations of our model due to both its simplifying assumptions and its generality. Some have already been mentioned in section 2.

- (1) The producers' growth does not depend on the total nutrient, N_T . This restricts our nutrient to one that is limiting only for the consumer. On the other hand, our model still supports a bifurcation sequence (Fig. 2) similar to LKE [26], KHE [24] and WKL [44]. This emphasizes the importance of the role of stoichiometry in the biomass conversion efficiency of the consumer, as opposed to the role of stoichiometry in producer growth.
- (2) From a technical standpoint, our use of the "Liebig law of the minimum" biomass conversion function leads to a nonsmooth model. Our equilibrium analysis relies on this selection. The model could be made smooth in a variety of ways, such as using the Kooijman approach of using synthesizing units [22] or Poisson arrival time models [31]. The additional realism of the smooth system, however, brings with it added analytic complexity of the model. Computation of our "case H " and "case L " coexistence equilibria would be analytically intractable in a smoothed version. We anticipate, however, that the only conclusions that would be affected are the fine details of the bifurcation diagrams, since nonsmoothness tends to collapse portions of such diagrams. The gross bifurcation behavior, however, can be expected to persist.
- (3) The fact that our model is closed to nutrients is an assumption that would require care to reproduce experimentally, but also one that contributes to the tractability of the model.
- (4) Foraging in our model is assumed to be nonpreferential: consumption is proportional to the relative abundance of each producer. Preferential predation might lead to different results.

5.4. Other behaviors of our model

We remind the reader that our bifurcation analysis is dependent on the auxiliary parameters chosen for the study. We do not claim that we have provided a complete description of all possible behaviors, even in the one-producer reduced model. There are many parameters in equation (4) which we have not varied and which could possibly lead to different behavior. For example, in similar models we have studied, a first saddle-node bifurcation has been observed to take place *off* the limit cycle (no SNIC), resulting in a coexisting attracting limit cycle and attracting equilibrium. A later homoclinic bifurcation destroys the limit cycle and returns the equilibrium to the only attractor. Other choices of the parameters in our model could lead to other scenarios.

As we indicated in the Ecological Implications subsection above, our bifurcation analysis can be viewed as a paradigm for studying many specific systems. Identification of species specific parameters, and recomputation of bifurcation diagrams such as those in Fig. 5 would be the first step in such a study.

6. Conclusions

The model developed and studied in this paper can be thought of as a simple Lotka-Volterra model of two competing producers and one consumer, altered to model the stoichiometric effects of food (producer) quality on consumer growth. The producers grow logistically. Stoichiometric limitation is modeled only by restricting the conversion efficiency from producer to consumer biomass. The stoichiometric effect is thus focussed on this mechanism. The model's nutrient uptake term, being proportional to both available nutrient and to producer growth, differs from the nutrient uptake in some other models, but does not appear to produce new dynamical behavior. See Diehl, Appendix A [7] for similar observations about the limited effect of varying nutrient uptake assumptions.

The main goal in our analysis has been to determine the response of the system to increased carbon (b_1 and b_2) and nutrient (N_T) enrichment. Consistent with many stoichiometric models, the overall effect of including stoichiometric constraints is to prevent enrichment from leading to large amplitude producer-consumer oscillations; especially with a fixed nutrient pool, there is not enough nutrient to support large populations. More specifically, in both the reduced single producer model, and the full two-producer model, the response of the system to enrichment (b , or b_1 and b_2 , respectively) leads to roughly the same bifurcation sequence as observed in previous stoichiometric studies with a single producer [26, 44] where carrying capacity was directly varied. This is true even though the latter models include additional stoichiometric restrictions on producer growth. By envisioning one-parameter cuts – with fixed total nutrient N_T – through figure 3(a), one can see that the same qualitative bifurcation scenario might be expected as long as N_T is above a threshold value (for example above approximately 0.05 in the figure). The specific cut exhibited in Fig. 2 is one example. A comparison of Fig. 3(a) with Fig. 8(a) shows that increasing nutrient uptake affects the system in a manner similar to increasing the total nutrient.

In the two-producer model, the large scale bifurcation scenario due to carbon enrichment (heading radially out from the origin in and Fig. 5(a),(b) or Fig. 9) is similar to the single-producer reduced model: no life, producer without consumer, coexistence, cycle coexistence, cycle replaced by new (low nutrient) equilibrium, and finally loss of consumer due to low producer stoichiometry. In general, as one moves away from the diagonal in the producer growth space (b_1, b_2), the producer with the lower growth rate eventually goes extinct in a transcritical bifurcation involving either an equilibrium or a periodic cycle. The details of the coexistence of one versus both producers, illustrated in Fig. 5(a),(b) or Fig. 9, is new to this study. This is especially interesting because it reveals some nonintuitive possibilities. It can be seen from the figures that there are, for example, straight line paths with positive slope (corresponding to enrichment) where the system goes from coexistence of all three species, to the loss of one producer, and back to coexistence. Features like the existence of interior periodic cycles without interior equilibria are also of dynamical interest.

To summarize, paying attention to stoichiometry in population models can drastically change predicted population behavior. This study adds to the understanding of the role of stoichiometry, especially in the restrictions on coexistence of a consumer which preys on more than one producer.

Acknowledgements

The authors would like to thank the referees for their valuable comments and suggestions.

7. Appendix

7.1. Numerical Methods

The bifurcation diagrams in this paper were computed using a variety of analytic and numerical methods.

- Figure 2. Most curves were plotted using *Mathematica 6.0* along with the explicit expressions for the equilibria in section 3. The exceptions were the curves for the “case L ” coexistence equilibria (red) and the curves representing the periodic limit cycles extrema (purple). For the case L coexistence equilibria, *Mathematica* was used (*FindRoots*) to determine $(P_1C)_L$ as a solution to the cubic equation (5). The other components were then calculated using the previously determined P_1 value. For the limit cycle extrema (purple), *Mathematica* was used to compute numerical solutions (*NDSolve*) from time 0 through time 2000. The numerical solutions were then processed from time 1000 through time 2000 to determine the extrema corresponding to each solution component. Steps of size 0.1 in b_1 were used.
- Figure 3. The transcritical bifurcation curves (blue) were computed by setting the consumer component of the coexistence equilibrium to zero. The Hopf curve (red) was computed by setting the real part of an eigenvalue of the equilibrium point to zero. The saddle-node curve (green) was computed using equation (5): they corresponded to extrema of the cubic in P_1 . The dashed lines – boundaries between low and high nutrient cases – were computed by solving for equilibria which also satisfied the stoichiometric condition that $Q/q = \alpha$.
- Figure 5. Bifurcation curves were mostly computed in a manner similar to the techniques described for Fig. 3. There were two exceptions. The “interior” Hopf curve was determined using *Mathematica* (*ContourPlot*) to solve for equilibria with eigenvalues that had zero real part. The curves representing transcritical bifurcations between side hyperplane cycles and interior cycles (cyan), forming part of the boundary of the $(P_1P_2C)_L$ cycle region in parts (b),(c),(d), were computed differently. To approximate these curves, numerical solutions to equation (3) were computed using *Mathematica* from time 0 to 6000. Newton’s method was then used to converge to a value of b_2 , given a value of b_1 , for which the coordinates for either P_1 or P_2 were zero.
- Figure 7. Methods were analogous to those used to compute Fig. 2.
- Figure 8. Methods for part (a) were analogous to methods for Fig. 3. Methods for parts (b) and (c) were analogous to methods for Fig. 5.

7.2. Additional bifurcation details

In this section we provide some additional details of descriptions of bifurcation diagrams presented in Figs. 5(a) and 7. In particular, we discuss bifurcations of unstable equilibria rather than just bifurcations involving attractors. While these bifurcations might not be as important ecologically, understanding them helps to understand the complete mathematical bifurcation structure, and following bifurcations of unstable equilibria often leads to bifurcations which *are* ecologi-

cally significant.

Figure 9. Figure 9 is an embellished version of Fig. 5(a). Solid lines separate regions which correspond to different attractors. The regions are labelled by the associated attractor, exactly as they are in Fig. 5(a). New to this figure are the dashed lines, corresponding to bifurcations of unstable equilibria, which subdivide these regions. We observe no regions of bistability for our choice of auxiliary parameters, so the labelling scheme is unique. From numerical work with similar models, however, we expect that certain parameter sets could allow bistability, with, for example, a coexistence equilibrium and a P_1P_2 equilibrium both being stable. There are three regions that allow for coexistence of all three species: $(P_1P_2C)_H$, P_1P_2C -cycle, and $(P_1P_2C)_L$. All other regions have behavior that can be described by a “reduced” model, without one of the three species.

We denote by O the region $(0 \leq b_1 \leq d_{P_1})$ and $(0 \leq b_2 \leq d_{P_2})$. The region is not labelled in Fig. 5(a) or Fig. 9; it is too small to see clearly. We did not provide time series for region O either; the consumer and both producers go extinct for this set of parameters.

For low values of b_2 (less than about 0.05), increasing b_1 leads to a sequence identical to that described for the one-producer model in Fig. 2. This is because the growth rate for producer P_2 is not sufficient to allow its survival. So the model reduces to a one-producer model. A vertical path for $0 \leq b_1 \leq 0.05$ results in a symmetric sequence of bifurcations but with $P_1 = 0$. A path along the diagonal results in a similar sequence but with both producers existing. The most interesting new feature is the transition from coexistence close to the diagonal to the extinction of P_1 as we move toward the b_2 axis, and the analogous extinction of P_2 as we move toward the b_1 axis. All these transitions occur as some form of a transcritical bifurcation – either the crossing of an equilibrium (across curve segment \overline{gf}) or \overline{cde} or a limit cycle (across \overline{fc}) from an “interior” attractor to a “ $P_2 = 0$ ” attractor.

Note the blue transcritical wedge boundaries \overline{rj} and $\overline{rj'}$. These bound the region of coexistence of the two producers without a consumer. Our region of coexistence of all three species turns out to be a subset of this wedge. The wedge is solid when it separates regions without a consumer (\overline{rg} and $\overline{rg'}$ in Fig. 9 and the line segments separating $(P_1P_2)_L$ from P_{1L} and P_{2L} in Fig. 5(b)), and dashed when it subdivides a region with a consumer (line segments \overline{gj} and $\overline{g'j'}$). Figure 9 includes several more dashed bifurcation lines: vertical ones which correspond to bifurcations in the $P_2 = 0$ “side hyperplane” and horizontal ones which correspond to bifurcations in the $P_1 = 0$ “side hyperplane.” The extension of the horizontal line at $b_2 = 0.05$ to the right of $b_1 = 0.05$ is not displayed. This does not involve any attractor, and in fact is only an ecologically significant bifurcation in the absence of both P_1 and C . The symmetric part of $b_1 = 0.05$ is also not displayed. All horizontal and vertical bifurcation lines actually extend indefinitely, but we have trimmed them both to keep Fig. 5(c) from further clutter, and to emphasize the connection between the side hyperplane bifurcations and the corresponding interior bifurcations. For example, the $P_2 = 0$ side hyperplane nonsmooth saddle-node (line \overline{kda}) is displayed only up to the point a , where it connects with the interior nonsmooth saddle-node (line $\overline{aa'}$).

Other dashed curves indicate equilibrium bifurcations not involving an attrac-

tor: a transcritical bifurcation of the unstable $(P_1P_2C)_H$ equilibrium from the interior of the phase space (P_1, P_2 and C all positive) to $P_2 = 0$ as we pass from region $\{ff'b'b\}$ to region $\{fbc\}$. A similar transition occurs from region $\{b'ba'a\}$ to region $\{abc\}$. Curve \overline{ca} denotes a transcritical bifurcation of a different unstable equilibrium from the interior to $P_2 = 0$. Recall that there are up to three interior equilibria: the original equilibrium which underwent a Hopf bifurcation across $\overline{ff'}$, and two additional equilibria born in the SNIC saddle-node bifurcation across $\overline{cbb'c'}$. A count of interior equilibria yields one in region $\{ff'b'b\}$, none in region $\{bcf\}$, three in region $\{bb'a'a\}$, two in region $\{abc\}$, and one in the rest of region $(P_1P_2C)_L$. Region $\{bcf\}$ is especially noteworthy because there exists an interior limit cycle, but no interior equilibrium.

Figure 7. This figure can be placed in context by looking at the $b_2 = 2$ path in Fig. 9. We will walk through the one-parameter cut from low to high b_1 and identify attractors first. Then we will describe the extra curves corresponding to nonattracting equilibria and candidate equilibria (in Fig. 7(d)). For low b_1 values, P_2 and C coexist on an attracting periodic limit cycle in region P_2C cycle. The solid magenta lines denote the extrema of this cycle. This is consistent with single producer analysis: the point $(b, N_T) = (2.0, 0.1)$ is in the PC -cycle region of Fig. 3(a). Note that the phase values of the extrema of the limit cycle do not change as b_1 is increased because P_1 is not yet enriched enough to survive. There is a transcritical crossing of periodic limit cycles at $b_1 \approx 1.38$. Producer N_1 now survives along with P_2 and C on an interior limit cycle (solid purple extrema). The interior limit cycle is destroyed in a SNIC bifurcation at $b_1 \approx 2.405$. The saddle-node is best illustrated in Fig. 7(b) where the solid red curve shows the attracting equilibrium $(P_1P_2C)_L$. At $b_1 \approx 4.28$, producer P_1 “outcompetes” producer P_2 , and P_2 goes extinct in a transcritical bifurcation. Not shown in any of the Fig. 7 diagrams, but apparent in the black dotted $b_2 = 2$ cut displayed in Fig. 5(b), the consumer is lost in the paradox of enrichment transcritical bifurcation at $b_1 \approx 14.2$.

Dashed lines correspond to unstable equilibria, either saddles or sources. Two of the dashed line segments correspond to interior equilibria: dashed blue in region $Cycle_a$, and dashed red in the first subregion of $(P_1P_2C)_L$. The dashed blue equilibrium is born in a $P_1 = 0$ transcritical bifurcation (see Fig. 7(a) at $b_1 \approx 1.62$), and dies in a $P_2 = 0$ transcritical bifurcation (see Fig. 7(b) at $b_1 \approx 2.38$). The red dashed equilibrium is born in the saddle-node bifurcation already mentioned above at $b_1 \approx 2.405$, and dies in a $P_2 = 0$ transcritical bifurcation at $b_1 \approx 2.6$. Both bifurcations are best viewed in Fig. 7(b).

Two additional side hyperplane equilibria are plotted: green dashed for $(P_1)_H$, and pink for $(P_2C)_H$. The $(P_1)_H$ monoculture is included mainly for Fig. 7(a), to show that all coexistence P_1 values are below the P_1 monoculture value. The pink dashed $(P_2C)_H$ side hyperplane equilibrium is included only to better see the transcritical bifurcation between subregions $Cycle_b$ and $Cycle_a$. See Fig. 7(b) or 7(c). We chose not to display the analogous connecting $P_2 = 0$ orbit at the transcritical bifurcation between regions $Cycle_a$ and $Cycle_b$ because its continuation would further complicate the diagrams.

As we did in Fig. 2(d), we show extra dotted curves denoting “candidate” equilibria in Fig. 7(d). The only difference in interpretation of the dotted lines in the two figures is that in the former, the dotted candidates are *mathematically*

unrealized because they don't satisfy the "consistency check", while in the latter, portions of the dotted lines are *ecologically* unrealizable because at least one component is negative. The part the dotted red curve that is above the γ value of 0.1 and the part of the dotted blue curve that is below γ are candidates which are unrealized for both reasons.

7.3. Mathematical bifurcation notes

The two-parameter bifurcation diagrams in this paper naturally raise the question of the identification of codimension-two bifurcation points wherever more than one codimension-one bifurcation curve cross or come together. Many of the codimension-two bifurcations in this paper are nonstandard because of the prevalence of transcritical bifurcations. These are nongeneric in bifurcation theory except in the presence of "invariant planes." Others are nonstandard because they involve nonsmooth changes. We identify below all bifurcation points in Fig. 3(a) and 5(c) where codimension-one bifurcation curves either cross or come together. "Trivial" crossings, which correspond to the crossing of two codimension-one bifurcation curves that do not interact in the same region of phase space, are denoted as bifurcation one \times bifurcation two.

- Figure 3(a):
 - (1) Point (a) is a nonsmooth \times transcritical point. A smooth approximation would eliminate this point.
 - (2) Point (b) is also a nonsmooth \times transcritical point. A smooth approximation would eliminate this point as well.
 - (3) Point (c) is a nonsmooth saddle-node/Hopf point. Based on bifurcation diagrams computed for previous research [34, 35], we expect a smooth approximation to resolve the bifurcation diagram into saddle-node curve with a codimension-two cusp, and a codimension-two Takens-Bogdanov point. The nonsmoothness in our model appears to collapse these two codimension-two points together.
- Figure 5(c):
 - (1) Points (r) and (g) are double transcritical bifurcation points.
 - (2) Point (f) is a transcritical/Hopf point.
 - (3) Point (b) is a SNIC \times transcritical point.
 - (4) Point (c) is a SNIC/transcritical point. This should have the same local unfolding as the saddle-node/transcritical point identified in [12].
 - (5) Point (a) is a nonsmooth saddle-node/transcritical point. A smooth approximation should resolve this into a smooth saddle-node/transcritical bifurcation like point (c).
 - (6) Point (d) is a nonsmooth saddle-node \times transcritical point.

Analysis of the double transcritical point and the transcritical/Hopf point should be especially tractable. This would allow us to better understand the nature of solutions for parameters in a neighborhood of the corresponding points in our bifurcation diagrams.

Table 1. Table of Variables

Variables	Definitions	Variables	Definitions
P_1	Population Density of Producer P_1 (Carbon)	N_1	Nutrient Density of Producer P_1
P_2	Population Density of Producer P_2 (Carbon)	N_2	Nutrient Density of Producer P_2
C	Population Density of Consumer C (Carbon)	N_C	Nutrient Density of Consumer C
$Q_1 = \frac{N_1}{P_1}$	Stoichiometric Ratio of P_1	$Q_2 = \frac{N_2}{P_2}$	Stoichiometric Ratio of P_2
M	Mineralized Nutrient		

Table 2. Bifurcations between the adjacent regions in figures 2 and 3: one producer, one consumer

Regions	Type of Bifurcation	Involved Attractors	Non-Attractor Transitions
$O \rightarrow P_H$	Transcritical	$O \rightarrow P$	
$P_H \rightarrow (PC)_H$	Transcritical	$P \rightarrow (PC)_H$	
$(PC)_H \rightarrow PC\text{-cycle}$	Hopf	$(PC)_H \rightarrow PC\text{-cycle}$	
$PC\text{-Cycle} \rightarrow (PC)_L \{cde\}$	SNIC	$PC\text{-cycle} \rightarrow (PC)_L$	An unstable $(PC)_L$ is also created.
$(PC)_L \{cde\} \rightarrow (PC)_L \{bcef\}$	Non-Smooth Saddle-node		The unstable $(PC)_H$ and unstable $(PC)_L$ are eliminated.
$(PC)_L \{bcef\} \rightarrow P_L$	Transcritical	$(PC)_L \rightarrow P_L$	

Table 3. Bifurcations between the adjacent regions in figures 5 and 7: two producers, one consumer

Regions	Type of Bifurcation	Attractors	Non-Attractor Transitions
$O \rightarrow (P_1P_2)_H$	Transcritical	$O \rightarrow (P_1P_2)$	
$O \rightarrow P_{1H}$	Transcritical	$O \rightarrow (P_1)$	
$P_{1H} \rightarrow (P_1P_2)_H$	Transcritical	$(P_1) \rightarrow (P_1P_2)$	
$(P_1P_2)_H \rightarrow (P_1P_2C)_H$	Transcritical	$(P_1P_2) \rightarrow (P_1P_2C)_H$	
$(P_1)_H \rightarrow (P_1C)_H$	Transcritical	$(P_1) \rightarrow (P_1C)_H$	
$(P_1C)_H \rightarrow (P_1P_2C)_H$	Transcritical	$(P_1C)_H \rightarrow (P_1P_2C)_H$	
$(P_1P_2C)_H \rightarrow Cycle_a$	Hopf	$(P_1P_2C)_H \rightarrow Interior\ cycle$	
$(P_1C)_H \rightarrow PIC\text{-Cycle}$	Hopf	$(P_1C)_H \rightarrow P_1C\text{-cycle}$	
$PIC\text{-cycle} \rightarrow Cycle_b$	Transcritical	$P_1C\text{-cycle} \rightarrow Interior\ cycle$	
$Cycle_b \rightarrow Cycle_a$	Transcritical		$(P_1C)_H \rightarrow (P_1P_2C)_H$
$Cycle_a \rightarrow (P_1P_2C)_L \{abb'a'\}$	SNIC	Interior cycle \rightarrow Stable $(P_1P_2C)_L$	Unstable $(P_1P_2C)_L$ is created.
$Cycle_b \rightarrow (P_1P_2C)_L \{abc\}$	SNIC	Interior cycle \rightarrow $(P_1P_2C)_L$	Unstable $(P_1P_2C)_L$ is created.
$P_1C - Cycle \rightarrow (P_1C)_L \{cdkm\}$	SNIC	$P_1C - cycle \rightarrow (P_1C)_L$	Unstable $(P_1C)_L$ is created.
$(P_1C)_L \{cdkm\} \rightarrow (P_1P_2C)_L \{acd\}$	Transcritical	$(P_1C)_L \rightarrow (P_1P_2C)_L$	
$(P_1P_2C)_L \{abb'a'\} \rightarrow (P_1P_2C)_L$	Non-Smooth Saddle-node		Unstable $(P_1P_2C)_H$ and unstable $(P_1P_2C)_L$ are eliminated.
$(P_1P_2C)_L \{abb'a'\} \rightarrow (P_1P_2C)_L \{abc\}$	Transcritical		$(P_1P_2C)_H \rightarrow (P_1C)_H$
$(P_1P_2C)_L \{abc\} \rightarrow (P_1P_2C)_L \{acd\}$	Transcritical		$(P_1P_2C)_L \rightarrow (P_1C)_L$
$(P_1P_2C)_L \{acd\} \rightarrow (P_1P_2C)_L$	Non-Smooth Saddle-node		Unstable $(P_1C)_H$ and unstable $(P_1C)_L$ are eliminated.
$(P_1C)_L \{cdkm\} \rightarrow (P_1C)_L \{edk\}$	Non-Smooth Saddle-node		Unstable $(P_1C)_H$ and unstable $(P_1C)_L$ are eliminated.
$(P_1C)_L \{cdkm\} \rightarrow (P_1P_2C)_L \{acd\}$	Transcritical	$(P_1C)_L \rightarrow (P_1P_2C)_L$	
$(P_1C)_L \{jedk\} \rightarrow (P_1P_2C)_L \{edaa'd'e'\}$	Transcritical	$(P_1C)_L \rightarrow (P_1P_2C)_L$	
$(P_1P_2C)_L \rightarrow (P_1P_2)_L$	Transcritical	$(P_1P_2C)_L \rightarrow (P_1P_2)$	
$(P_1C)_L \rightarrow (P_1)_L$	Transcritical	$(P_1C)_L \rightarrow (P_1)$	
$(P_1)_L \rightarrow (P_1P_2)_L$	Transcritical	$P_1 \rightarrow (P_1P_2)_L$	

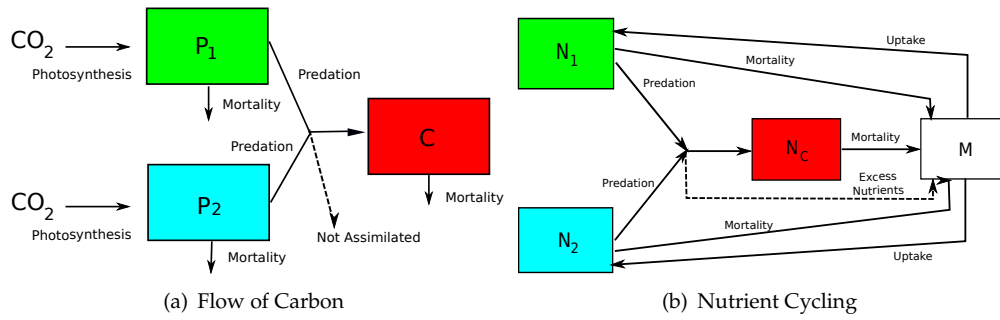


Figure 1. Two-Producer-One-Consumer Flow Charts: Carbon Flow and Nutrient Cycling

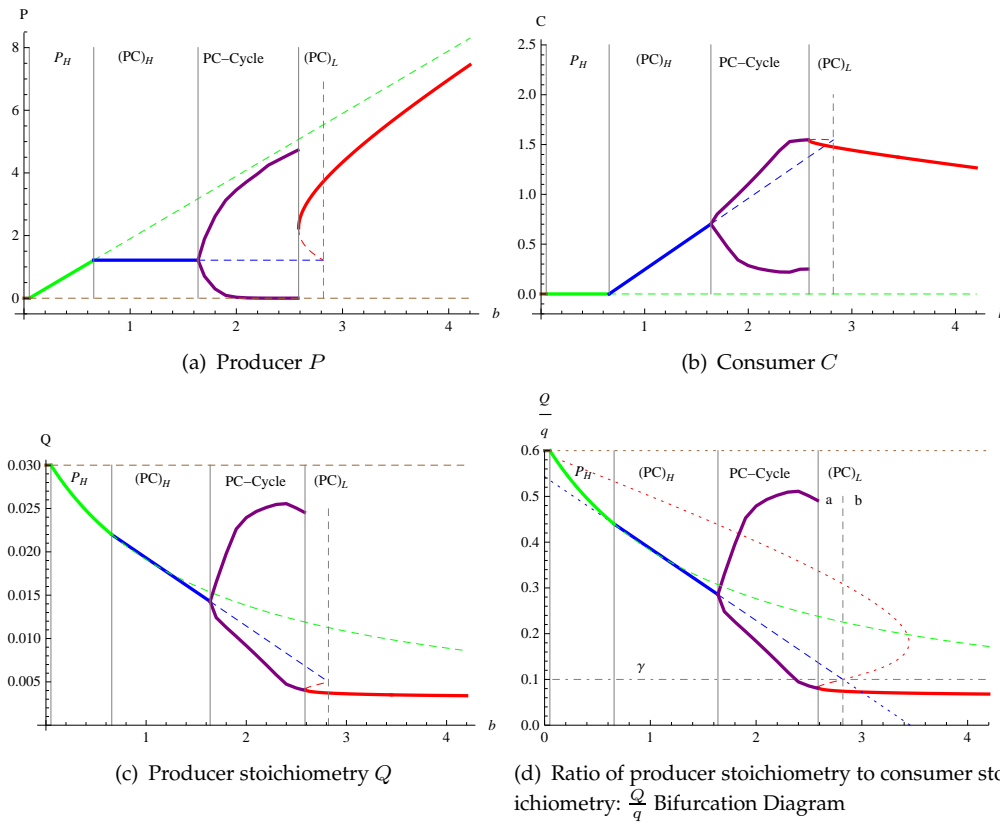
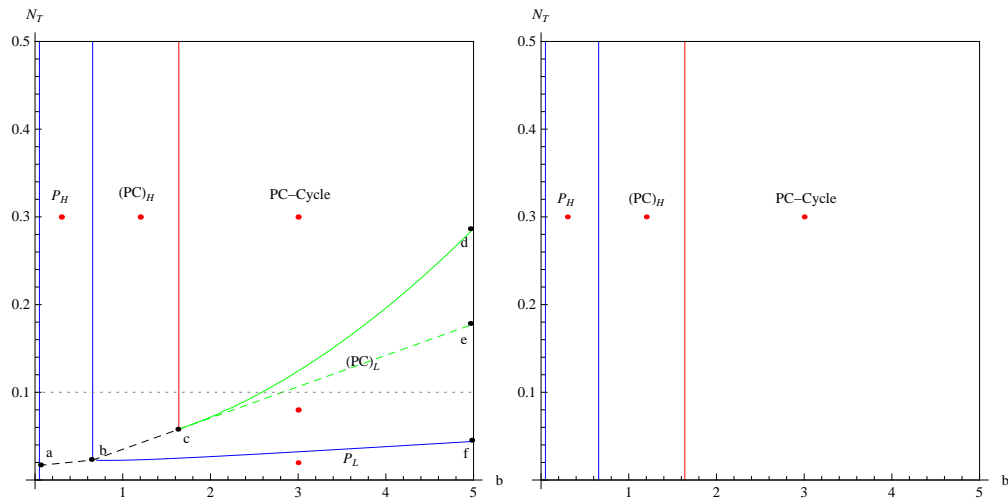


Figure 2. One-parameter bifurcation diagrams for the reduced One-Producer-One-Consumer Model of equation (4). (a),(b),(c) Traditional projections of the respective phase variable versus the producer growth rate b . Attracting equilibria and extrema of attracting limit cycles are illustrated with solid curves; unstable equilibria are illustrated with dashed lines. Vertical lines indicate bifurcations; parameter regions are labeled by the corresponding attractor. Bifurcations and approximate b values are: transcritical (0.05), transcritical (0.65), Hopf (1.63), SNIC (2.6), and nonsmooth saddle-node (2.82). (d) Producer stoichiometry to consumer stoichiometry: $\frac{Q}{q}$ Bifurcation Diagram; dotted blue and red curves denote unrealized candidate equilibria. See text for more explanation.



(a) Bifurcation diagram for eq. (4); see Fig. 4 for representative time series corresponding to the red dot in each region. (b) Bifurcation diagram without stoichiometric effects: eq. (4) with $\min(\gamma, \frac{Q}{q})$ replaced by γ .

Figure 3. Two-parameter bifurcation diagrams in b and N_T for the one-producer-one-consumer model. Solid curves indicate a change of attractor; dashed curves do not. Bifurcations are color coded: blue for transcritical, red for Hopf, green for saddle-node, dashed green for nonsmooth saddle-node of unstable equilibria, dashed black for change in classification between high- and low-nutrient producer equilibrium. See table 2 for bifurcations between adjacent regions. See text for more explanation.

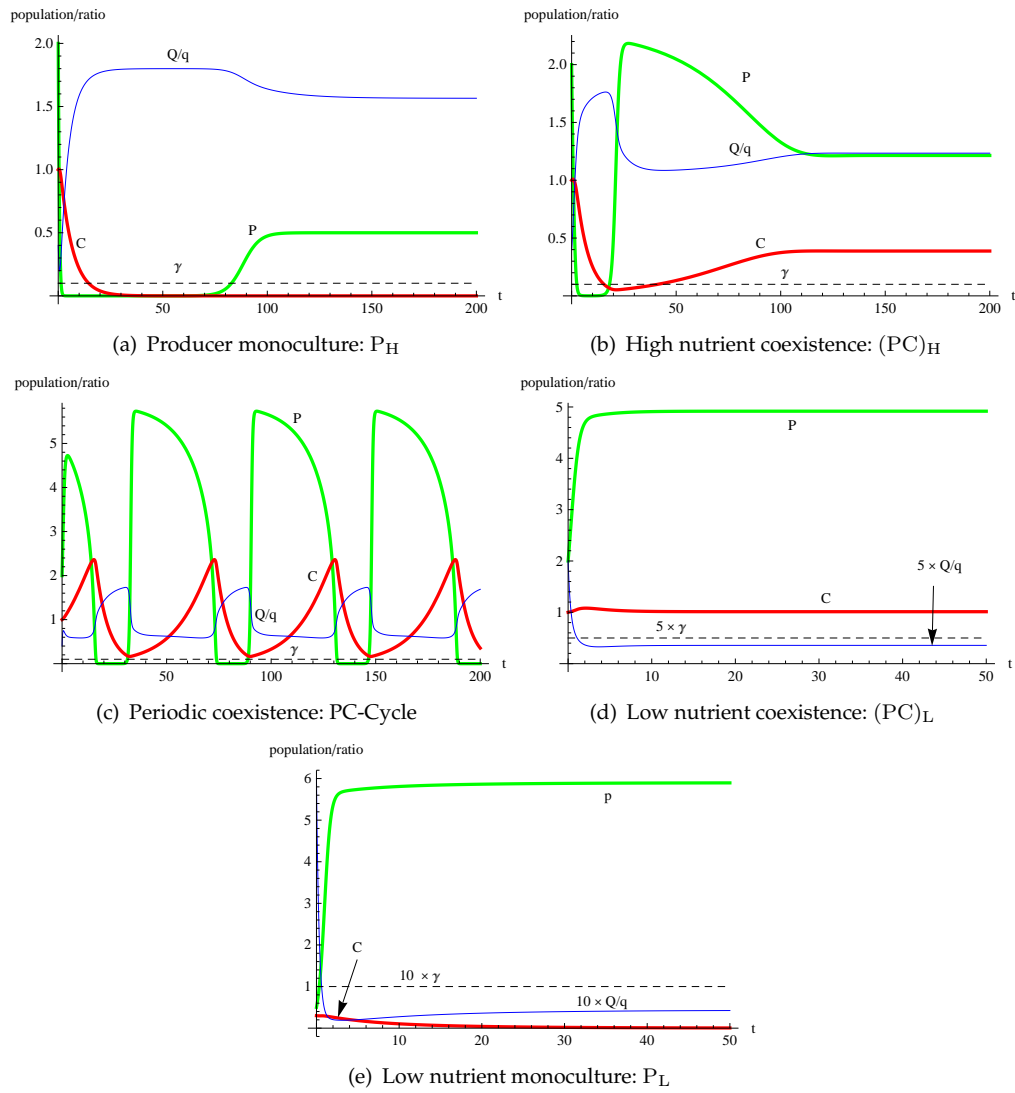
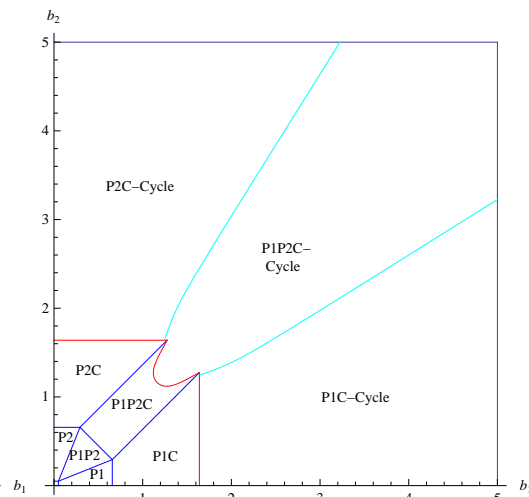
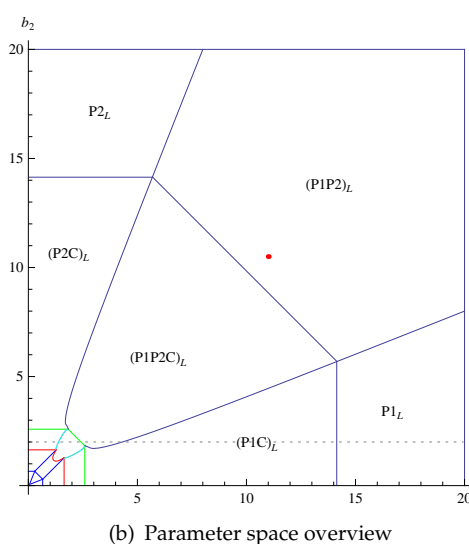
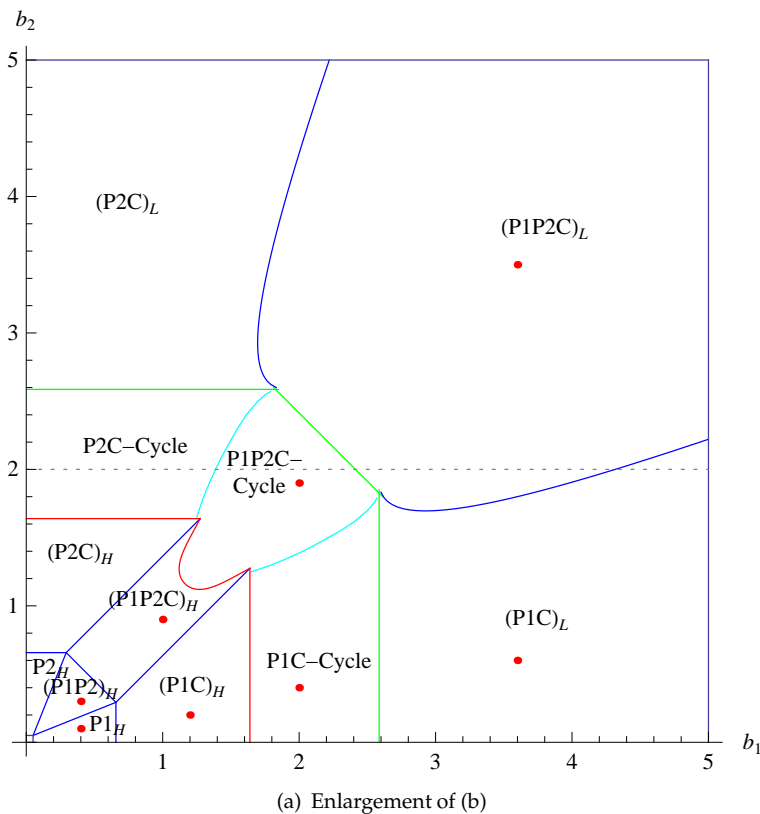


Figure 4. Representative time series corresponding to the red dot parameter values in Fig. 3(a). Green is for the producer P ; red is for the consumer C ; blue is for the producer's (rescaled) ratio Q/q ; the dashed line is the same rescaling $\times \gamma$: when $Q/q \geq \gamma$, the producer is "high" nutrient, and when $Q/q < \gamma$, the producer is "low" nutrient. (a) $b = 0.3$, $N_T = 0.3$, and initial $(P, C, Q) = (2, 1, 0.02)$; (b) $b = 1.2$, $N_T = 0.3$, and initial $(P, C, Q) = (2, 1, 0.02)$; (c) $b = 3$, $N_T = 0.3$, and initial $(P, C, Q) = (2, 1, 0.02)$; (d) $b = 3$, $N_T = 0.08$, and initial $(P, C, Q) = (2, 1, 0.02)$; (e) $b = 3$, $N_T = 0.02$, and initial $(P, C, Q) = (0.5, 0.3, 0.003)$.



(c) Same as (a) but without stoichiometry: replace $\min(\gamma, \frac{P_1 Q_1 + P_2 Q_2}{P_1 + P_2})$ with γ in equation (3). Standard Rosenzweig-MacArthur behavior but for two producers: limit cycle behavior persists for large b_1 and/or b_2 .

Figure 5. Two-parameter bifurcation diagrams, b_2 versus b_1 , for the Two-Producer-One-Consumer Model of equation (3). Regions are labelled according to the associated attractor. Bifurcations are color coded: blue for transcritical, red for Hopf, green for saddle-node (nonsmooth), and cyan for transcritical bifurcations of limit cycles. Dotted black lines correspond to the $b_2 = 2$ one-parameter cut of Fig. 7. Representative time series for the red dot parameter values are displayed in Fig. 6. See a summary of the attractors in each region and bifurcations between regions in table 3. See the text here and in 7.2 for more explanation.

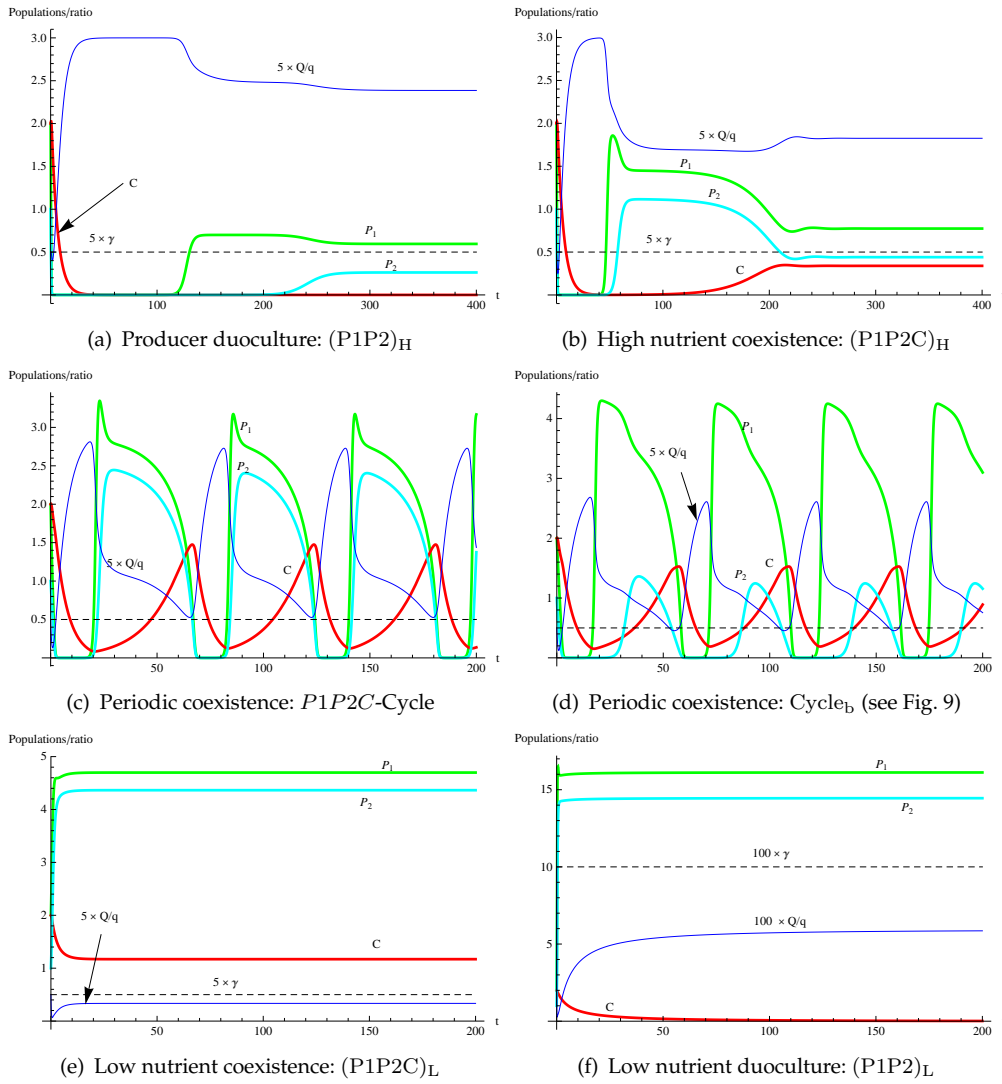


Figure 6. Representative time series corresponding to parameter regions in Fig. 5. The time series in $P1_H$, $(P1C)_H$, $P1C - \text{Cycle}$, $(P1C)_L$, and $P1_L$ are similar to the ones in Fig. (4). Green is for the producer P_1 ; cyan is for the producer P_2 ; red is for the consumer C ; blue is for the producers combined (rescaled) ratio Q/q where $Q = \frac{P_1 Q_1 + P_2 Q_2}{P_1 + P_2}$; the dashed line is the same rescaling $\times \gamma$: when $Q/q \geq \gamma$, the producer is “high” nutrient, and when $Q/q < \gamma$, the producer is “low” nutrient. (a) $b_1 = 0.4, b_2 = 0.3, N_T = 0.1$, and initial $(P_1, P_2, C, Q_1, Q_2) = (2, 1, 2, 0.005, 0.005)$; (b) $b_1 = 1, b_2 = 0.9, N_T = 0.1$, and initial $(P_1, P_2, C, Q_1, Q_2) = (2, 1, 2, 0.005, 0.005)$; (c) $b_1 = 2, b_2 = 1.9, N_T = 0.1$, and initial $(P_1, P_2, C, Q_1, Q_2) = (2, 1, 2, 0.005, 0.005)$; (d) $b_1 = 2.3, b_2 = 1.7, N_T = 0.1$, and initial $(P_1, P_2, C, Q_1, Q_2) = (2, 1, 2, 0.005, 0.005)$; (e) $b_1 = 3.6, b_2 = 3.5, N_T = 0.1$, and initial $(P_1, P_2, C, Q_1, Q_2) = (2, 1, 2, 0.005, 0.005)$; (f) $b_1 = 11, b_2 = 10.5, N_T = 0.1$, and initial $(P_1, P_2, C, Q_1, Q_2) = (2, 1, 2, 0.005, 0.005)$.

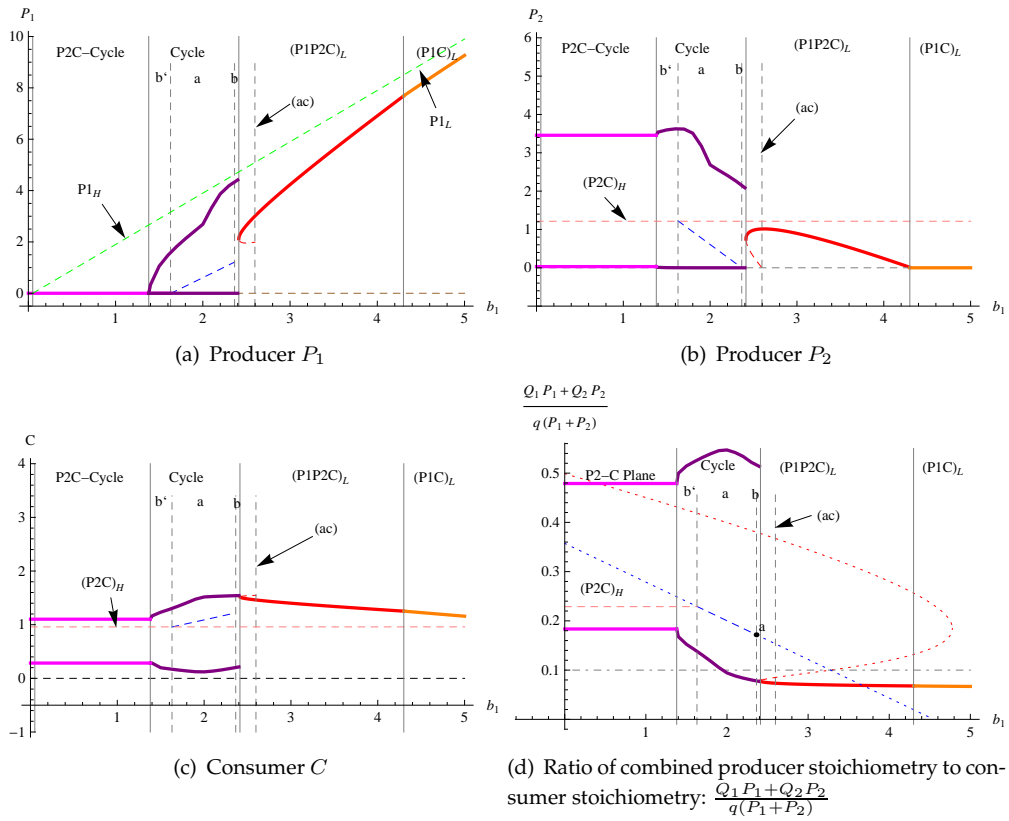
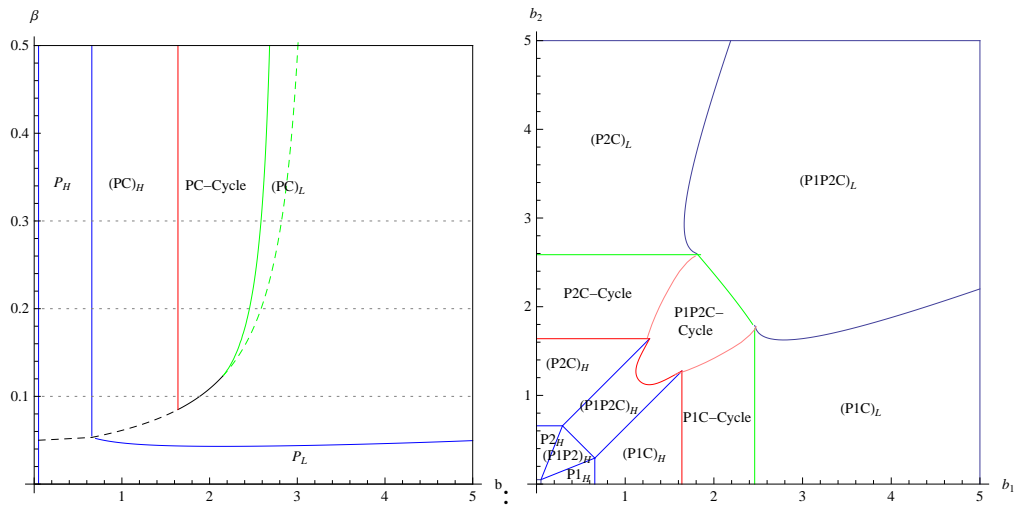
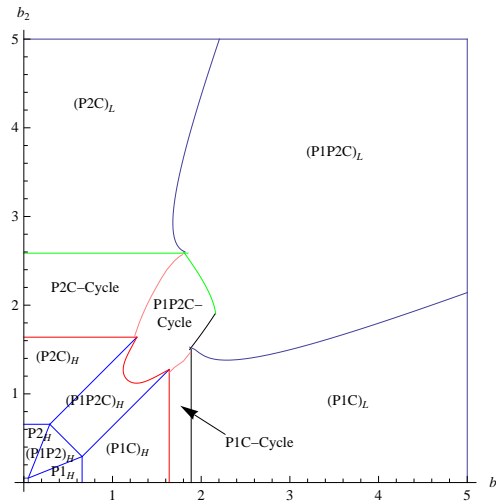


Figure 7. One-parameter bifurcation diagrams in b_1 for the Two-Producer-One-Consumer Model of equation (3); see the corresponding $b_2 = 2.0$ path in Figs. 5(a), (b), or Fig. 9. Solid lines denote attracting equilibria or extrema of attracting limit cycles; dashed lines denote unstable equilibria; dotted lines in (d) denote unrealized candidate equilibria. Solid vertical lines denote bifurcations of the attractor; dashed vertical lines denote bifurcations not involving the attractor (all are transcritical bifurcations of equilibria); the label (ac) corresponds to the crossing of curve \overline{ac} in Fig. 9. See the Appendix for a more detailed explanation.



(a) β versus b bifurcation diagram for the one-producer-one-consumer model of equation (4); compare with Fig. 3(a): increase in uptake β is similar to increase in total nutrient, N_T .
 (b) Same as Fig. 5(a), except for $\beta_1 = .2$. The diagram is slightly asymmetrical.



(c) Same as Fig. 5(a), except for $\beta_1 = .1$. The diagram is clearly asymmetrical.

Figure 8. Bifurcation diagrams for varying producer nutrient uptake rate β (in (a)) or β_1 (in (b) and (c)). Solid curves denote a change in attractor; dashed curves do not. Bifurcations are blue for transcritical, red for Hopf, green for saddle-node, cyan for transcritical bifurcation of limit cycles. Dashed green in (a) is a nonsmooth saddle-node; dashed black in (a) is a change in classification of the producers' combined stoichiometry; solid black in (a) and (c) is for an unnamed nonsmooth bifurcation.

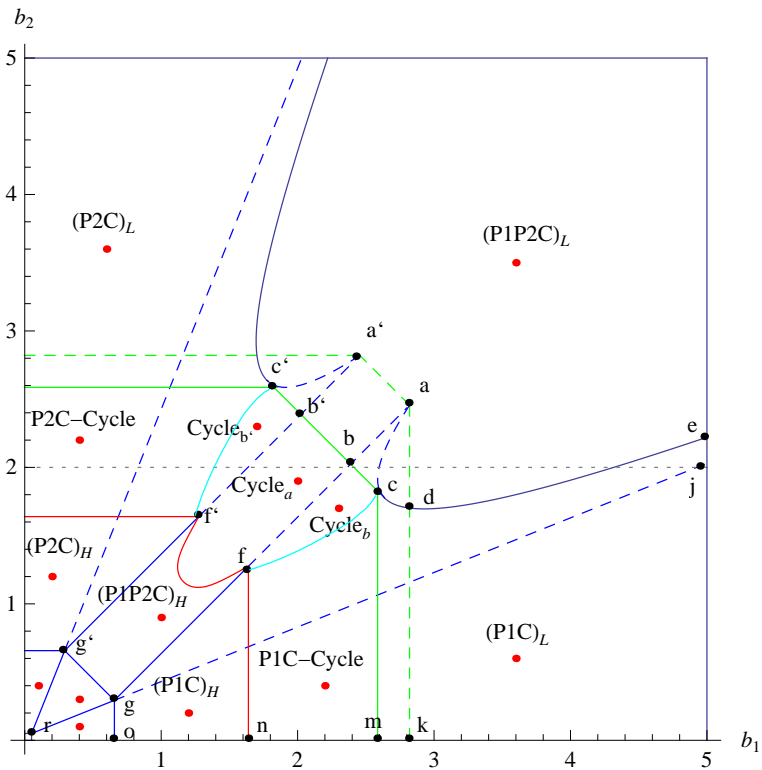


Figure 9. Detailed version of Fig. 5(a). Solid lines indicate a change of attractor; dashed lines indicate bifurcations involving unstable equilibria. Dotted black line at $b_2 = 2$ correspond to the one-parameter cut of Fig. 7. Representative time series corresponding to red dot parameter values are displayed in Fig. 6. See a summary of the attractors in each region and bifurcations between regions in Table 3. See the text in the Appendix for more explanation.

References

- [1] T. Andersen, *Pelagic nutrient cycles: Herbivores as sources and sinks*, Springer-Verlag, New York (1997).
- [2] T. Andersen, J. Elser, and D.O. Hessen, *Stoichiometry and population dynamics*, *Ecology Letters* 7 (2004), pp. 884–900.
- [3] F.J. Ayala, M.E. Gilpin, and J.G. Ehrenfield, *Competition between species: theoretical models and experimental tests*, *Theoretical Population Biology* 4 (1973), pp. 331–356.
- [4] G. Belovsky, *Diet optimization in a generalist herbivore: the moose*, *Theoretical Population Biology* 14 (1978), pp. 105–134.
- [5] J.M. Chase, P.A. Abrams, J.P. Grover, S. Diehl, P. Chesson, R.D. Holt, R.M. Nisbet, and T.J. Case, *The interaction between predation and competition: a review and synthesis*, *Ecology Letters* 5 (2002), pp. 302–315.
- [6] W.R. DeMott, R.D. Gulati, and K. Siewertsen, *Effects of phosphorus-deficient diets on the carbon and phosphorus balance of daphnia magna*, *Limnol. Oceanogr.* 43 (1998), pp. 1147–1161.
- [7] S. Diehl, *Paradoxes of enrichment: Effects of increased light versus nutrient supply on pelagic producer-grazer systems*, *The American Naturalist* 169 (2007).
- [8] K.A. Dunning, M. Kyle, Y. Kuang, and J.J. Elser, *A mathematical and empirical analysis of stoichiometric effects of light intensity on daphnia dynamics and coexistence*, *Journal of Young Investigators* 19 (2008).
- [9] J.J. Elser and J. Urabe, *The stoichiometry of consumer-driven nutrient recycling: Theory, observations, and consequences*, *Ecology* 80 (1999), pp. 735–751.
- [10] M. Fan, I. Loladze, K. Yang, and J. Elser, *Dynamics of a stoichiometric discrete producer-grazer model*, *Journal of Difference Equations and Applications* 11 (2005), pp. 347–365.
- [11] M.E. Gilpin, *Spiral chaos in a predator prey model* 113 (1973).
- [12] W.G. Graves, B.B. Peckham, and J. Pastor, *A bifurcation analysis of a differential equations model for mutualism*, *Bulletin of Mathematical Biology* 68 (2006), pp. 1837–1850.
- [13] J. Grover, *Stoichiometry, herbivory, and competition for nutrients: Simple models based on planktonic ecosystems*, *J. Theoretical Biology* 214 (2002), pp. 599–618.
- [14] J.P. Grover, *The impact of variable stoichiometry on predator-prey interactions: A multinutrient approach*, *The American Naturalist* 162 (2003), pp. 29–43.
- [15] J.P. Grover, *Predation, competition, and nutrient recycling: a stoichiometric approach with multiple nutrients*, *Journal of Theoretical Biology* 229 (2004), pp. 31–43.
- [16] J.P. Grover and R.D. Holt, *Disentangling resource and apparent competition: Realistic models for plant-herbivore communities*, *Journal of Theoretical Biology* 191 (1998), pp. 353–376.
- [17] J. Huisman and F. Weissing, *Competition for nutrients and light in a mixed water column: a theoretical analysis*, *The American Naturalist* 46 (1995), pp. 536–564.
- [18] K. Keesting, *Some features of feeding, respiration and energy conversion of daphnia magna*, *Hydrobiologia* 59 (1978), pp. 113–120.
- [19] D.A. Kiefer and C.A. Atkinson, *Cycling of nitrogen by plankton: A hypothetical description based upon efficiency of energy conversion*, *Journal of Marine Research* 42 (1984), pp. 655–675.
- [20] S.S. Kilham, D.A. Kreeger, S.G. Lynn, C.E. Goulden, and L. Herrera, *Combo: a defined freshwater culture medium for algae and zooplankton*, *Hydrobiologia* 377 (1998), pp. 147–159.
- [21] B. Kooijman and S. Kooijman, *Invading species can stabilize simple trophic systems*, *Ecological Modelling* 133 (2000), pp. 57–72.
- [22] S. Kooijman, *The synthesizing unit as model for the stoichiometric fusion and branching of metabolic fluxes*, *Biophysical Chemistry* 73 (1998), pp. 179–188.
- [23] N.R. Kretzschmar M. and E. McCauley, *A predator-prey model for zooplankton grazing on competing algal populations*, *Theoretical Population Biology* 44 (1993), pp. 32–66.
- [24] Y. Kuang, J. Huisman, and J. Elser, *Stoichiometric plant-herbivore models and their interpretation*, *Mathematical Biosciences and Engineering* 1 (2004), pp. 215–222.
- [25] L. Lin, *A stoichiometric model of two producers and one consumer*, Master’s thesis, University of Minnesota Duluth (2008).
- [26] I. Loladze, Y. Kuang, and J. Elser, *Stoichiometry in producer-grazer systems: Linking energy flow with element cycling*, *Bulletin of Mathematical Biology* 62 (2000), pp. 1137–1162.
- [27] I. Loladze, Y. Kuang, J. Elser, and W. Fagan, *Competition and stoichiometry: Coexistence of two predators on one prey*, *Theoretical Population Biology* 65 (2004), pp. 1–15.
- [28] C.R. Miller, Y. Kuang, W.F. Fagan, and J.J. Elser, *Modelling and analysis of stoichiometric two-patch consumer-resource system*, *Mathematical Biosciences* 189 (2004), pp. 153–184.
- [29] R. Moen, J. Pastor, and Y. Cohen, *Antler growth and extinction of the irish elk*, *Evolutionary Ecology Research* 1 (1999), pp. 235–249.
- [30] R. Nisbet, E. McCauley, A. De Roos, W. Murdoch, and W. Gurney, *Population dynamics and element recycling in an aquatic plant-herbivore system*, *Theoretical Population Biology* 40 (1991), pp. 125–147.
- [31] R.V. O’Neill, D.L. DeAngelis, J. Pastor, B.J. Jackson, and W.M. Post, *Multiple nutrient limitations in ecological models*, *Ecological Modelling* 46 (1989), pp. 147–163.
- [32] J. Pastor, *Mathematical ecology of populations and ecosystems*, Wiley-Blackwell (2008).
- [33] J. Pastor and Y. Cohen, *Herbivores, the functional diversity of plants, and cycling of nutrients in ecosystems*, *Theoretical Population Biology* 51 (1997), pp. 165–179.
- [34] B.B. Peckham, *The necessity of the hopf bifurcation for periodically forced oscillators with closed resonance regions*, *Nonlinearity* 3 (1990), pp. 261–280.
- [35] B.B. Peckham and J. Montaldi, *Real continuation from the complex quadratic family: fixed-point bifurcation sets*, *Internat. J. Bifur. Chaos, Appl. Sci. Engrg.* 10 (2000), pp. 391–414.
- [36] S. Richman, *The transformation of energy by daphnia pulex*, *Ecological Monographs* 28 (1958), pp. 273–291.
- [37] M.L. Rosenzweig and R.H. MacArthur, *Graphical representation and stability conditions for predator-prey interactions*, *American Naturalist* 97 (1963), pp. 209–223.
- [38] L.B. Slobodkin, *Energetics in daphnia pulex populations*, *Ecology* 40 (1959), pp. 232–243.
- [39] R. Sterner and J. Elser, *Ecological stoichiometry*, Princeton University Press (2002).
- [40] G. Sui, M. Fan, I. Loladze, and K. Yang, *The dynamics of a stoichiometric plant-herbivore model and its discrete*

- analog*, Mathematical Biosciences and Engineering 4 (2007), pp. 1–18.
- [41] J. Urabe and R. Sterner, *Regulation of herbivore growth by the balance of light and nutrients*, Proceeding of the National Academy of Sciences of the United States of America 93 (1996), pp. 8465–8469.
- [42] R. Vance, *Predation and resource partitioning in one predator – two prey model communities*, The American Naturalist 112 (1978), pp. 797–813.
- [43] P. Waltman, *Competition models in population biology*, CBS-NSF Regional Conference Series in Applied Mathematics, SIAM, Philadelphia, PA. (1983), pp. 797–813.
- [44] H. Wang, Y. Kuang, and I. Loladze, *Dynamics of a mechanistically derived stoichiometric producer-grazer model*, Journal of Biological Dynamics 00 (2007), pp. 1–11.
- [45] L. Zimmermann, *A producer-consumer model with stoichiometry*, Technical Report TR 2006-5, University of Minnesota Duluth, Department of Mathematics and Statistics, Duluth, MN, 2006.